Separation of the σ_L and σ_T contributions to the production of hadrons in electroproduction

H. Avakian[ab], L. Elouadrhiri, G. Gavalian, V. Kubarovsky, N. Sato, and X. Wei

Thomas Jefferson National Accelerator Facility, Newport News, Virginia 23606

A. Afanasev

The George Washington University, Washington, DC 20052

F. Benmokhtar

Duquesne University, Pittsburgh, PA 15282

K.T. Brinkmann

II. Physikalisches Institut der Universität Gießen, 35392 Gießen, Germany

R. Capobianco

University of Connecticut, Storrs, Connecticut 06269 and
Argonne National Laboratory, Lemont, Illinois 60439

S. Diehl

II. Physikalisches Institut der Universität Gießen, 35392 Gießen, Germany and
University of Connecticut, Storrs, Connecticut 06269

C. Dilks

Duke University, Durham, North Carolina 27708-0305

T.B. Hayward[ac], K. Joo, A. Kim, and U. Shrestha[ad]

University of Connecticut, Storrs, Connecticut 06269

S. Kuhn

Old Dominion University, Norfolk, Virginia 23529

P. Rossi

Thomas Jefferson National Accelerator Facility, Newport News, Virginia 23606 and

[a] Co-spokesperson

[b] Contact: `avakian@jlab.org`

[c] Contact: `timothy.hayward@uconn.edu`

[d] Contact: `ushrestha@uconn.edu`

INFN, Laboratori Nazionali di Frascati, 00044 Frascati, Italy

M. Scott and M. Zurek

Argonne National Laboratory, Lemont, Illinois 60439

A clear separation and evaluation of the contributions of longitudinal photons is a necessary step to understanding systematic uncertainties in the phenomenology used to extract underlying 3D parton distributions from measurements of multiplicities and azimuthal asymmetries in the semi-inclusive and hard exclusive production of hadrons, including $ep \to e'hX$ and $ep \to e'hhX$. We propose an addition to the Run Group K experiments in Hall B, focusing on performing an in-depth analysis of the cross sections to produce hadrons in lepto-scattering. By comparing the obtained results with those from Run Group A, conducted at a higher beam energy, and performing a Rosenbluth separation, we aim to disentangle the contributions from transversely and longitudinally polarized photons. The Rosenbluth separation is performed empirically by measuring the semi-inclusive leptoproduction cross section at a set of kinematics corresponding to the same photon 4-momentum Q^2 and longitudinal momentum x, but at different ratios of longitudinal to transverse photon polarization ϵ. This requires measurements at different combinations of incident electron energy and scattering angle. While moderately accurate measurements of the ratio R_{DIS} of longitudinal to transverse cross section exist for inclusive deep inelastic scattering, there have been no measurements of R_{SIDIS} for the SIDIS process. Our study aims to fill this gap in knowledge and provide valuable insights into the nucleon structure and quark-gluon dynamics.

CONTENTS

I. INTRODUCTION

A. Semi-inclusive Deep Inelastic Scattering

Semi-inclusive deep inelastic scattering (SIDIS), where an electron scatters off a nucleon target at a high enough energy such that it can be described by scattering off a single parton in the target [1], is a powerful tool for investigating nucleon structure and quark-gluon dynamics. Measurements of the SIDIS cross sections for various hadron production processes provide essential information about the underlying quark distributions and their interactions within the nucleon. Different structure functions that contribute to the fully differential SIDIS cross section in the one-photon-exchange approximation contain various convolutions of twist-2 or higher twist parton distribution functions (PDFs) and fragmentation functions (FFs) that are multiplied by specific kinematic prefactors [2]. The SIDIS cross section for an unpolarized beam and target can be expressed in terms of longitudinal and transverse contributions from virtual photons along with their interference terms [2–4]:

$$\frac{d\sigma}{dxdQ^2dzdP_T^2d\phi} = \frac{\pi\alpha^2}{x^2Q^4}\frac{(2x+\gamma^2)}{(1+\gamma^2)}K(y)\left(F_{UU,T} + \epsilon F_{UU,L} + \sqrt{2\epsilon(1+\epsilon)}\cos\phi F_{UU}^{\cos\phi} + \epsilon\cos(2\phi)F_{UU}^{\cos(2\phi)}\right). \tag{1}$$

The structure functions (SFs), represented by $F_{UU,T}$, $F_{UU,L}$, $F_{UU}^{\cos\phi}$ and $F_{UU}^{\cos(2\phi)}$, play a crucial role in describing the nucleon's internal structure as they encode information about the quark distributions and their interactions within the nucleon. Subscripts in the structure functions $F_{UU,LU,...}$, specify the beam (first index) and target (second index) polarization, U, L for the unpolarized and longitudinally polarized case, respectively. The depolarization factors represent the fraction of the initial electron polarization that is transferred to the virtual photon, which influences the virtual photon's polarization state and are described by the variable

$$K(y) = 1 - y + y^2/2 + \gamma^2y^2/4, \qquad \varepsilon = \frac{1 - y - \frac{1}{4}\gamma^2y^2}{1 - y + \frac{1}{2}y^2 + \frac{1}{4}\gamma^2y^2}, \tag{2}$$

with γ, x, y and Q^2 defined below. Additional variables, relevant for all SIDIS analyses, are given by

$$Q^2 = -q^2, \tag{3}$$

$$W^2 = (P+q)^2, \tag{4}$$

$$\nu = \frac{q \cdot P}{M} = E - E', \tag{5}$$

$$x = \frac{Q^2}{2P \cdot q} = \frac{Q^2}{2M\nu}, \tag{6}$$

$$y = \frac{P \cdot q}{P \cdot \ell} = \frac{\nu}{E}, \tag{7}$$

$$z = \frac{P \cdot P_h}{P \cdot q} = \frac{E_h}{\nu}, \tag{8}$$

$$\gamma = \frac{2Mx}{Q} = \frac{Q}{\nu}, \tag{9}$$

$$P_T = P_h \sin\theta_{\gamma h}, \tag{10}$$

The four-momentum of the exchanged virtual photon is defined as $q = l - l'$ such that $Q^2 = -q^2$ is the hard scale of the process (the virtuality of the exchanged photon). Conversely, W is the mass of the virtual photon-target system (the "hadronic mass"). If the electron beam has energy E and the scattered electron has energy E' then ν is defined as the difference between these two quantities. The variables x, y, and z are, respectively, the fraction of target momentum carried by the struck quark, the fraction of beam energy transferred to the virtual photon and the fraction of the virtual photon energy carried by the final state hadron. The quantity γ describes the relationship between the energy transferred to the struck quark and the energy of the virtual photon. If $\theta_{\gamma h}$ is the angle between the hadron momentum and the virtual photon momentum, then P_T is the projection of P_h perpendicular to the virtual photon direction.

SIDIS studies using CLAS12 with the capability of precision measurements of multiparticle final-state observables in a multidimensional space in x, Q^2, z, P_T would allow for the separation of different structure functions, as well as the separation of different contributions to relevant structure functions, which is critical for the interpretation and full understanding of the complex nature of nucleon structure properties and the hadronization processes.

B. Contributions to the SIDIS cross section

The study of the SIDIS cross section provides invaluable insight into the structure of nucleons. However, the complexity of these cross sections poses significant experimental and phenomenological challenges. With up to 18 structure functions to consider [2] (depending on the relevant degrees of freedom, such as beam and target polarizations), each structure function offers unique information about quark-gluon dynamics in the nucleon. These structure functions have intricate kinematic dependencies, such as x, Q^2, and P_T, and measuring each requires the full dependence of ϕ of the reaction and, in some cases, the dependence of ϵ. The importance of separating the structure functions cannot be overstated.

Table I provides insight into the complexity of SIDIS reactions by listing the structure functions with their corresponding characteristics. The twist of the correlation functions in the low transverse momentum region and the power counting of collinear factorization in the high transverse momentum region are indicated. The asterisk signifies mismatches of the power counting between the high- and low- transverse-momentum regions, implying the contribution of different mechanisms to the production of observed hadrons. The last two columns show the ease of measuring the structure functions in JLab and the EIC. For instance, the prefactor and twist of the structure function $F_{LU}^{\sin\phi_h}$ make it a suppressed twist-3 effect at low transverse momentum, making it difficult to measure at the EIC. Furthermore, the evolution properties of the underlying TMDs can further reduce the signal, as in the case of $F_{UT,T}^{\sin(\phi_h-\phi_S)}$, which involves the Sivers function. The table also provides information on the expected magnitudes of the structure functions, based on Ref. [5].

A unique feature of the $F_{UU,L}$ structure function, which makes it very challenging for theory, is that while it is expected to be dominated by leading twist contributions at higher transverse momenta, it is twist 4 for low transverse momenta. In addition, SIDIS processes get significant contributions from exclusive and semi-exclusive processes, where the $F_{UU,L}$ is, in fact, the leading twist contribution, while the $F_{UU,T}$ structure function is normally sub-leading (in contrast to SIDIS). Separation of these contributions is not always straightforward, and for precision measurements will require detailed measurements of all the contributions of exclusive and semi-exclusive events to SIDIS through radiative processes.

It is expected that as $z \to 1$ (i.e. exclusive scattering) that the Q^2 dependence of $R_{\mathrm{SIDIS}} = F_{UU,L}/F_{UU,T}$ should change from $1/Q^2$ to Q^2. Experimental measurements at COMPASS on the deuteron [6] and the proton [7], at HERMES [8] and CLAS/CLAS12 [9, 10] have shown that $F_{UU}^{\cos 2\phi_h}$ is related in the perturbative limit to $F_{UU,L}$ [11], and $F_{UU}^{\cos\phi_h}$ arising from the interference between longitudinal and transverse photons (see Tab. I), can be very significant, with $\cos\phi_h$ as high as 30% [6–8]. A very strong signal for the structure function $F_{UT}^{\sin\phi_S}$ at large z has been observed by both the HERMES and COMPASS collaborations and also indicates possible large contributions from longitudinal photons.

One of the most interesting observations of the COMPASS experiment, made possible by the large statistics collected on the proton, is the Q^2-dependence of $\cos\phi_h$. Contrary to the expectations, according to which its size should decrease like $1/Q$, $\cos\phi_h$ is observed to increase in size with Q^2. Similar behavior was also observed for $\sin\phi_h$ by the CLAS12 collaboration [10]. Among the possible reasons for this trend could be the relative reduction of the denominator with Q^2 (which depends on $F_{UU,T}$ and $F_{UU,L}$ together). If that is the case, that will indicate very significant contributions from longitudinal photons, also dominating in certain kinematics, where the cosine modulations generated by the interference of longitudinal and transverse photons are more significant. That will make the evaluation of the contributions from longitudinal photons in the total cross section absolutely critical for the interpretation of all kind of azimuthal modulations, in particular at large z and P_T.

Since longitudinal photons can produce significant cross sections, the contribution of $F_{UU,L}$ cannot be overlooked in general, as it might also be substantial and necessary for an accurate extraction of $F_{UU,T}$. Since in the non-perturbative region it is expected to rise with P_T, its account can significantly improve the major limitations in phenomenological description of the SIDIS data at $P_T < 1.5$ GeV.

The $F_{UU,L}$, which represents the longitudinal component of the SIDIS cross section, can be computed at order α_S, where α_S is the QCD coupling, and leading twist. In the TMD-case, $F_{UU,L}$ can also be computed at high transverse momentum and is predicted to be equal to twice the structure function $F_{UU}^{\cos 2\phi}$ [11]. To gain further insight into the role of longitudinal structure functions in SIDIS reactions, one can estimate $F_{UU,L}$ at low transverse momentum using the approximation from Refs. [11, 12] where the transverse momentum distributions (TMDs) are extracted from data. Figure 1 shows predictions for the ratio $R = F_{UU,L}/F_{UU,T}$ based on the MAP22 and SV19 TMD analysis [13, 14], with sizable contributions that can reach up to 30-50%. Therefore, the contribution of $F_{UU,L}$ cannot be overlooked, as it can be substantial and necessary for an accurate interpretation of $F_{UU,T}$, which is connected with standard leading twist TMDs.

The interpretation of SIDIS data in terms of TMDs has been a significant challenge in recent years, as it involves multiple physical mechanisms that contribute to the production of hadrons in the final state. In the context of the recent string+$^3P_0$ model of polarized hadronization [15], it was shown that a deeper understanding of the spin dependence of hadronization will require studies of vector mesons (VM), and in particular for the production of ρ mesons. The contamination of the

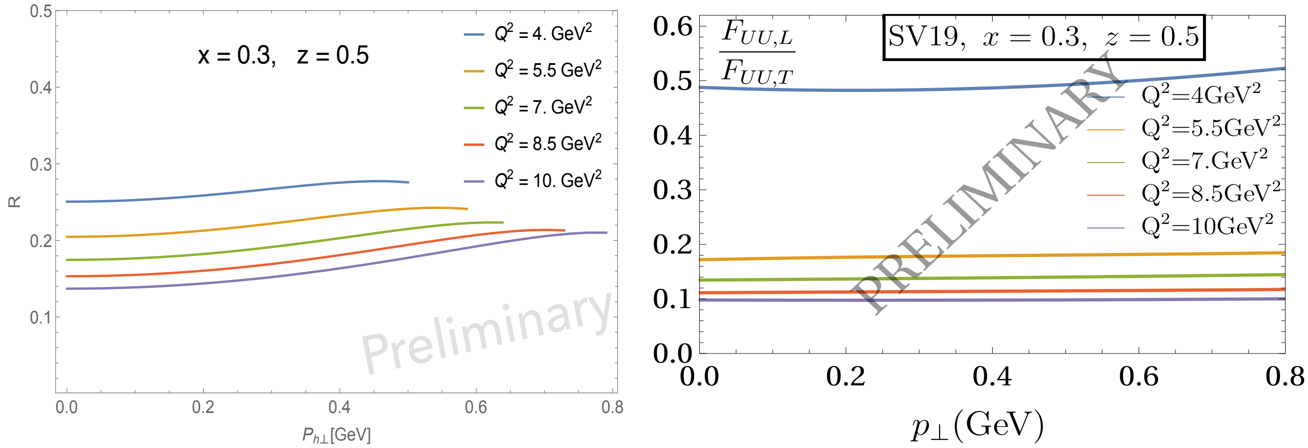

FIG. 1: Estimate of $R_{\mathrm{SIDIS}} = F_{UU,L}/F_{UU,T}$ at fixed values of x and z and for different values of Q^2 using MAP22 (left) and a simplified model (only u-quark) using SV19 (right).

ρ meson sample from decays of heavier resonances is also expected to be negligible according to simulations, meaning that these mesons carry information mostly on the direct mechanisms of quark fragmentation. Radiative effects in electroproduction [16] may also introduce additional systematics in phenomenological extractions, requiring detailed measurements of all involved SFs. Contributions to $F_{UU,T}$ and $F_{UU,L}$ from different mechanisms will also lead to dependence of radiative corrections, making the separation of different mechanisms important for the interpretation of the SIDIS data.

Measurements of R will require evaluation of systematics associated with initial and final state hadron mass corrections in SIDIS [17]. Multi-dimensional measurements of SIDIS cross section as a function of Q^2, enabling studies of subleading power corrections originating from higher-twist parton correlations would allow to quantify the systematics of factorized description of hadron production in SIDIS.

Structure function	γ^* helicity	prefactor	low-P_{hT} twist	low-P_{hT} PDF	high-P_{hT} calculation twist	order	power	JLab	EIC
$F_{UU,T}$	TT	1	2	f_1	2	α_s	$1/P_{hT}^2$	+	+
$F_{UU,L}$	LL	ϵ	4		2	α_s	$1/Q^2$	+	=
$F_{UU}^{\cos\phi_h}$	LT	$\sqrt{2\epsilon(1+\epsilon)}$	3	$h,\ f^\perp$ + tw. 2	2	α_s	$1/(QP_{hT})$	+	=
$F_{UU}^{\cos 2\phi_h}$	TT	ϵ	2	$h_1^\perp$	2	α_s	$1/Q^2$ [*]	+	+
$F_{LU}^{\sin\phi_h}$	LT	$\sqrt{2\epsilon(1-\epsilon)}$	3	$e,\ g^\perp$ + tw. 2	2	α_s^2	$1/(QP_{hT})$	+	−
$F_{UL}^{\sin\phi_h}$	LT	$\sqrt{2\epsilon(1+\epsilon)}$	3	$h_L,\ f_L^\perp$ + tw. 2	2	α_s^2	$1/(QP_{hT})$	+	=
$F_{UL}^{\sin 2\phi_h}$	TT	ϵ	2	$h_{1L}^\perp$	2	α_s^2	$1/Q^2$ [*]	+	=
F_{LL}	TT	$\sqrt{1-\epsilon^2}$	2	g_1	2	α_s	$1/P_{hT}^2$	+	=
$F_{LL}^{\cos\phi_h}$	LT	$\sqrt{2\epsilon(1-\epsilon)}$	3	$e_L,\ g_L^\perp$ + tw. 2	2	α_s	$1/(QP_{hT})$	+	−
$F_{UT,T}^{\sin(\phi_h-\phi_S)}$	TT	1	2	$f_{1T}^\perp$	3	α_s	$1/P_{hT}^3$	+	=
$F_{UT,L}^{\sin(\phi_h-\phi_S)}$	LL	ϵ	4		3	α_s	$1/(Q^2P_{hT})$	+	−
$F_{UT}^{\sin(\phi_h+\phi_S)}$	TT	ϵ	2	h_1	3	α_s	$1/P_{hT}^3$	+	=
$F_{UT}^{\sin(3\phi_h-\phi_S)}$	TT	ϵ	2	$h_{1T}^\perp$	3	α_s	$1/(Q^2P_{hT})$ [*]	=	−
$F_{UT}^{\sin\phi_S}$	LT	$\sqrt{2\epsilon(1+\epsilon)}$	3	$f_T,\ h_T,\ h_T^\perp$+ tw. 2	3	α_s	$1/(QP_{hT}^2)$	+	=
$F_{UT}^{\sin(2\phi_h-\phi_S)}$	LT	$\sqrt{2\epsilon(1+\epsilon)}$	3	$f_T^\perp,\ h_T,\ h_T^\perp$ + tw. 2	3	α_s	$1/(QP_{hT}^2)$	=	−
$F_{LT}^{\cos(\phi_h-\phi_S)}$	TT	$\sqrt{1-\epsilon^2}$	2	g_{1T}	3	α_s	$1/P_{hT}^3$	+	=
$F_{LT}^{\cos\phi_S}$	LT	$\sqrt{2\epsilon(1-\epsilon)}$	3	$g_T,\ e_T,\ e_T^\perp$ + tw. 2	3	α_s	$1/(QP_{hT}^2)$	=	−
$F_{LT}^{\cos(2\phi_h-\phi_S)}$	LT	$\sqrt{2\epsilon(1-\epsilon)}$	3	$g_T^\perp,\ e_T,\ e_T^\perp$ + tw. 2	3	α_s	$1/(QP_{hT}^2)$	=	−

TABLE I: Table of the SIDIS structure functions. The asterisks in the "power" column signify mismatches of the power counting between the high- and low- transverse-momentum regions. The "+/-/=" indicate the ability to measure SFs in the kinematics, where the valence quarks play a prominent role ($x > 0.1$), where "+" means measurable with certain assumptions, "=" means "possible but challenging", and "-" means "difficult".

C. Previous R_{SIDIS} Measurements

While moderately accurate measurements of the ratio R_{DIS} exist for the ratio of longitudinal to transverse cross sections for inclusive deep inelastic scattering, there are essentially no measurements of R_{SIDIS} for the SIDIS process. Previous measurements of pion electroproduction at moderate Q^2 and W were performed at the Cornell synchrotron in the 1970s at values of ϵ separated by less than 0.1 and averaged over ϕ and $P_T < 0.2$ GeV. These data allowed for the extraction of R_{SIDIS}, albeit with a very large uncertainty [18].

More recent SIDIS measurements at HERMES, COMPASS, and Jefferson Lab have assumed $R_{\text{SIDIS}} = R_{DIS}$, which is independent of z, P_T, and ϕ, as well as hadron and target nucleon identities. The assumption of $R_{\text{SIDIS}} = R_{DIS}$ introduces significant uncertainties when using SIDIS data to infer quark flavor and spin distributions. Given the origin of contributions from longitudinal photons [19], with an expected strong dependence on the transverse momentum of hadrons, that assumption is very likely to introduce significant systematics, practically uncontrolled at large non-perturbative transverse momenta. Incidentally, this region is where most of the disagreements were observed in phenomenological attempts to describe the data from HERMES and COMPASS. To address this issue and improve our understanding of nucleonic structure, it is crucial to obtain direct measurements of R_{SIDIS}.

Previous measurements of the structure function $F_{UU,L}$, have shown that this structure function is of the same order of magnitude as the structure function $F_{UU,T}$. R_{DIS} evaluated from the measurements of F_L in HERA using 3 beam energies, for $Q^2 \geq 3.5$ GeV^2 shows a constant behavior with $R = 0.260 \pm 0.050$ [20]. Similar results were obtained at JLab at lower beam energies [21]. In non-perturbative kinematics in SIDIS, particularly at relatively large transverse momenta, it is possible that this ratio can even exceed unity.

D. RGA Analysis of $\cos\phi$ and $\cos 2\phi$ Modulations

Semi-inclusive deep inelastic π^+ electroproduction has been studied with the CLAS12 detector at Jefferson Laboratory. The analyzed data was taken with a 10.6 GeV polarized electron beam, interacting with an unpolarized liquid hydrogen target and a negative (inbending) torus polarity. The statistics collected enable a high-precision study of the azimuthal moments $\cos\phi$ and $\cos 2\phi$ of the unpolarized cross sections. These azimuthal moments may probe the Boer-Mulders function, which describes the net transverse polarization of quarks inside an unpolarized proton, and the Cahn effect, which has a purely kinematic origin. In Fig. 2 some preliminary extractions of the 1D-unfolded ϕ distribution are shown for several z-P_T bins in one particular Q^2-x bin. At high P_T (top of the graph) the relative contributions of the $\cos\phi$ amplitude are much higher than $\cos 2\phi$, while at lower P_T the two amplitudes are similar in magnitude. The $\cos\phi$ amplitude, which corresponds to the so-called $d\sigma_{LT}/dt$ part of the cross section, receives significant contributions from longitudinal photons. At large transverse momenta both azimuthal moments increase, making proper separation of azimuthal modulations very important for precision measurements of the ϕ-independent SFs, such as $F_{UU,T}$ and $F_{UU,L}$. Studying their P_T dependence, where the RGA data already implies a changing R_{SIDIS} value with P_T, will be a main goal of this proposal.

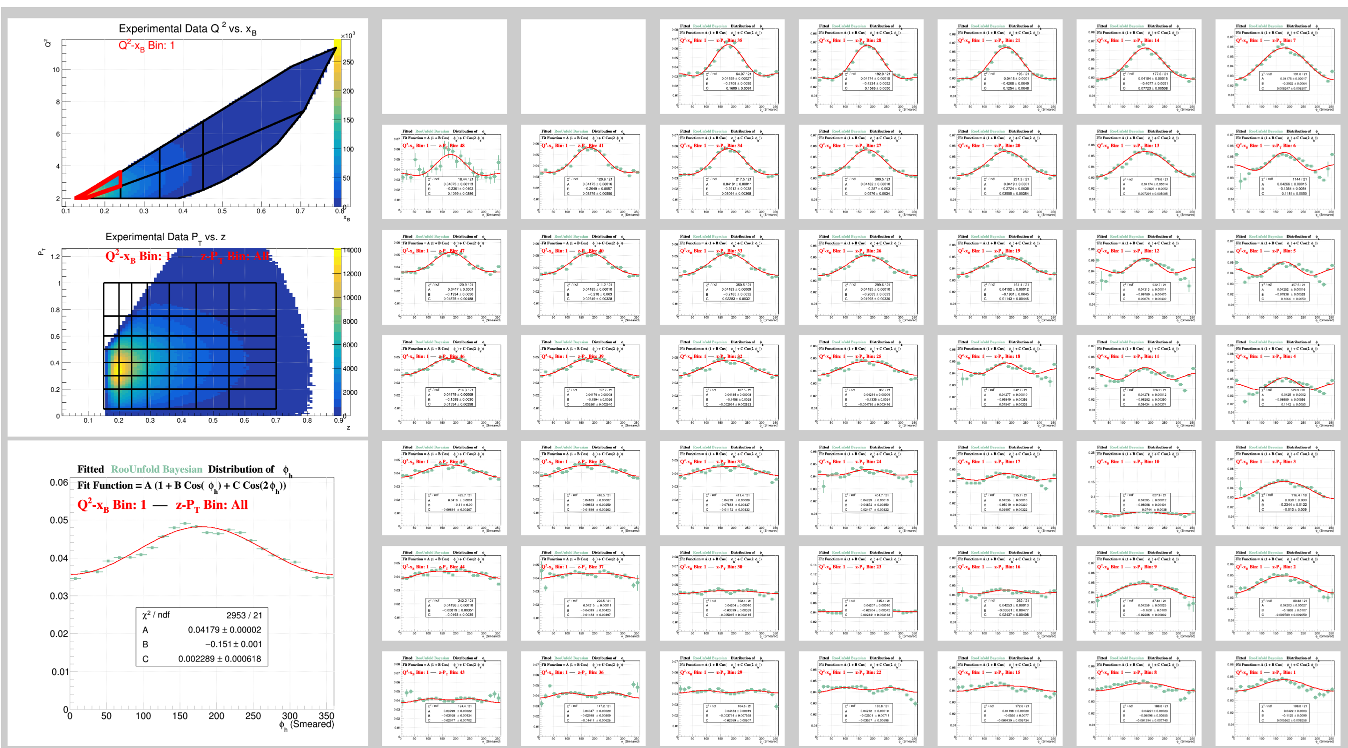

FIG. 2: **Preliminary** ϕ unfolded distributions for the $ep \to e'\pi^+X$ channel using the Bayesian Unfolding method. Plots show the distributions within Q^2-x Bin 1 (highlighted in red) and in each of the individual z-P_T bins (P_T increases from bottom to top and z increases from left to right). Each plot has been fitted with an equation of the form $A(1 + B\cos\phi + C\cos 2\phi)$, where $A = A_0(1 + \epsilon R_{\text{SIDIS}})$ for the purpose of this proposal.

II. EXPERIMENTAL SET UP

The proposed measurements will be conducted using the CLAS12 detector [22] in the previously approved RG-K configuration, following a similar approach to other approved SIDIS studies [23–28]. The CLAS12 system is an upgrade of the original CLAS detector and features a new dual magnetic field system. This system includes a superconducting solenoid magnet for momentum reconstruction within the polar angle range of 5° to 45°, and a torus magnet that allows for nearly complete 360° azimuthal coverage.

The CLAS12 detector is divided into six independent sectors, each providing one-sixth of the total azimuthal coverage. Additionally, the detector is separated into the Forward Detector (FD) and Central Detector (CD) systems. The FD of CLAS12 is responsible for detecting particles scattered at angles below approximately 35°. It comprises Cherenkov counters [29, 30], a dedicated ring imaging Cherenkov counter for pion/kaon discrimination [31], drift chambers [32], time-of-flight scintillators [33], and electromagnetic calorimeters [34].

On the other hand, the CD detects particles deflected at larger angles, ranging from approximately 35° to 125°. It consists of a silicon vertex tracker [35], a central time of flight system [36], and a central vertex tracker [37]. The solenoid used for the central tracker also serves to generate the magnetic field required for the polarized target.

III. MONTE CARLO

A. Description

The CLAS12 Fall 2018 RGA and RGK experimental configuration has been described in detail in GEMC [38], a GEANT4-based simulation package that offers the possibility to easily implement detectors in a complete GEANT simulation. The position of the detectors in Hall B has been matched to survey data, and a realistic map of the magnetic field has been generated to accurately reproduce the experimental setup. LUND generators were used to produce realistic final states that were read by GEMC version 4.3.2 and passed through CLAS12. The results of this process were cooked with COATJAVA version 6.5.3 and the reconstructed banks were added to the original generated banks for comparison. The generator used for SIDIS Monte Carlo analysis is clasdis [39], which is based on the PEPSI generator [40, 41], the polarized version of the well-known LEPTO generator [42].

B. MC Event Matching

In order to evaluate the effects of several systematics, such as bin migration effects, it is necessary to be able to match particles created in the Event Generator and "detected" particles after they have been processed by the GEMC detector simulation and particle reconstruction of CLAS12. Unfortunately, at the time of this proposal, no strict truth matching was included in the Monte Carlo process in order to be able to match tracks before and after reconstruction with full certainty. Instead, a requirement of matching electric charge (measured by curvature in the magnetic field) and restrictions on the lab frame angles of the tracks, $\Delta\phi < 6^\circ$ and $\Delta\theta < 2^\circ$, were used to pair generated and reconstructed particles. The effect of subtly altering this requirement by varying the strictness of the angular cuts was studied in the thesis of Timothy Hayward, p. 85 [43], in the RGA Common Analysis note [44] and in other CLAS12 SIDIS analysis. No dramatic dependence was observed and the differences correspond to sub-permil levels, which are much smaller than any uncertainties on the Monte Carlo models themselves. A requirement of matching particle identification is not enforced because this is one of the important systematics to study (e.g. the rate of kaons misidentified as pions).

C. Monte Carlo Smearing

It has been observed in previous CLAS12 analyzes that the Monte Carlo resolution is superior to that of reconstructed data. In the preliminary analysis of the $\cos\phi$ and $\cos 2\phi$ modulations of RGA data, a particle-dependent smearing function has been developed for electrons and pions to better mimic realistic resolution effects. Modifications were made using exclusive reactions within the data samples to match the widths of the ΔP distributions in both the experimental data and the Monte Carlo files. These methods have not been fully updated and checked for the lower beam energies but will be incorporated into the final analysis.

D. Data vs MC Comparison

The clasdis MC has repeatedly been shown to be an effective tool for describing CLAS12 SIDIS data. As we use Monte Carlo for the majority of our studies in this proposal, we provide several examples of comparisons between clasdis MC and existing CLAS12 data. In Fig. 3 the reconstructed clasdis MC is compared with collected CLAS12 RG-K data for 6.5 and 7.5 GeV. Excellent agreement is observed for the integrated samples. As further examples, comparisons between the collected RGA Fa18 outbending data and the clasdis MC are shown in Figs. 4-5.

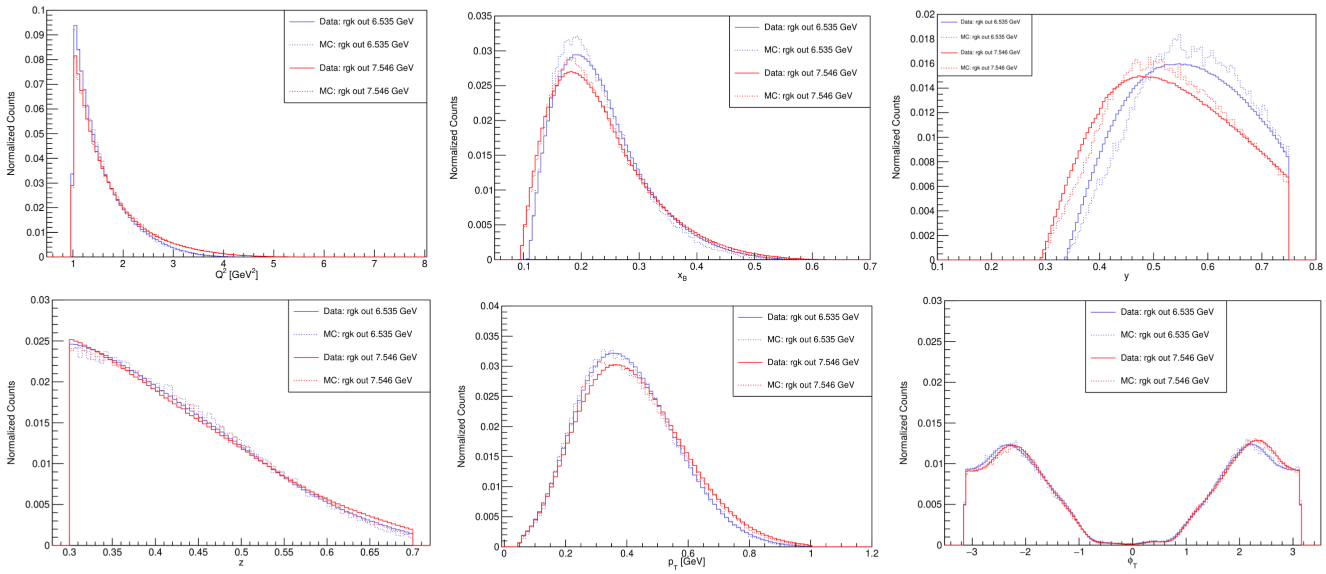

FIG. 3: Comparisons between the clasdis MC (dotted lines) and collected CLAS12 data (solid lines) for 6.5 GeV (blue) and 7.5 GeV (red). The top row shows relevant DIS variables (Q^2, x and y) and the bottom row shows relevant SIDIS variables (z, P_T and ϕ). The data sets have been normalized to the total number of π^+ in order to allow for a direct comparison of the shapes of the distributions.

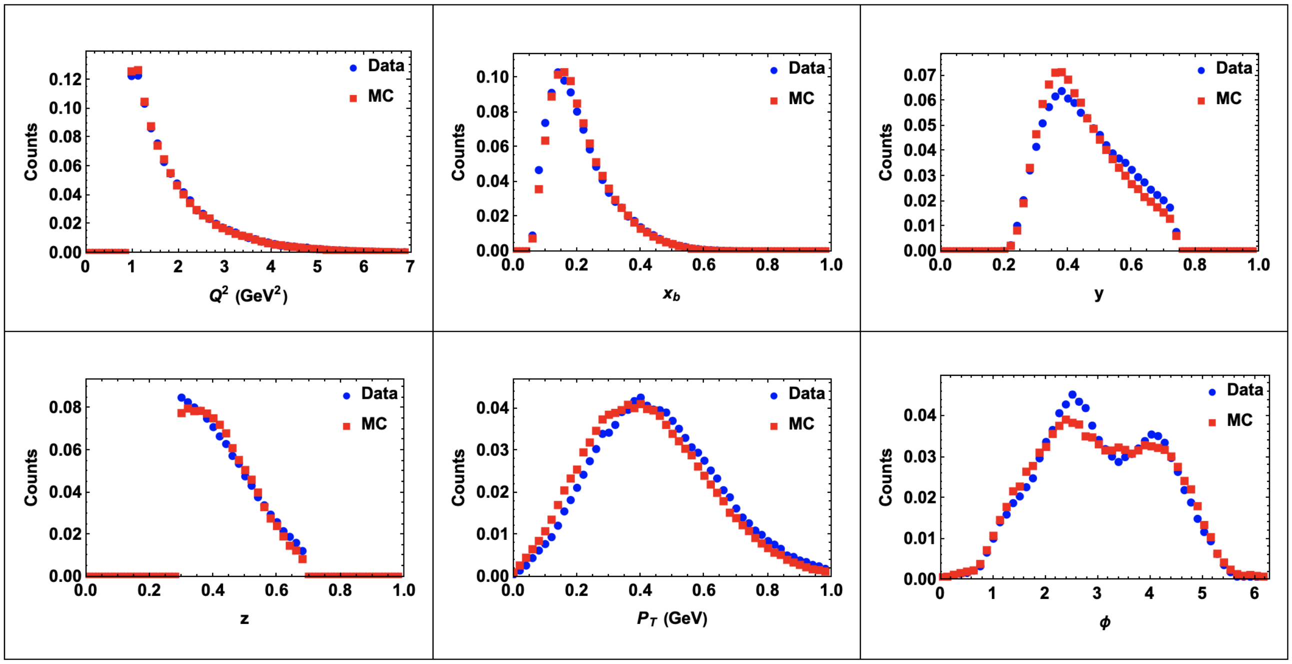

FIG. 4: Comparisons between the integrated outbending 10.6 GeV clasdis MC (red) and RGA Fall18 outbending 10.6 GeV data (blue) samples for Q^2, x, y, z, P_T and ϕ without resolution smearing. Good agreement is observed in general. Some slight differences are observed for the y and P_T distributions (the difference in ϕ can be explained by the lack of unpolarized modulations in the clasdis generator). The datasets have been normalized to the total number of π^+ in order to allow a direct comparison of the shapes of the distributions.

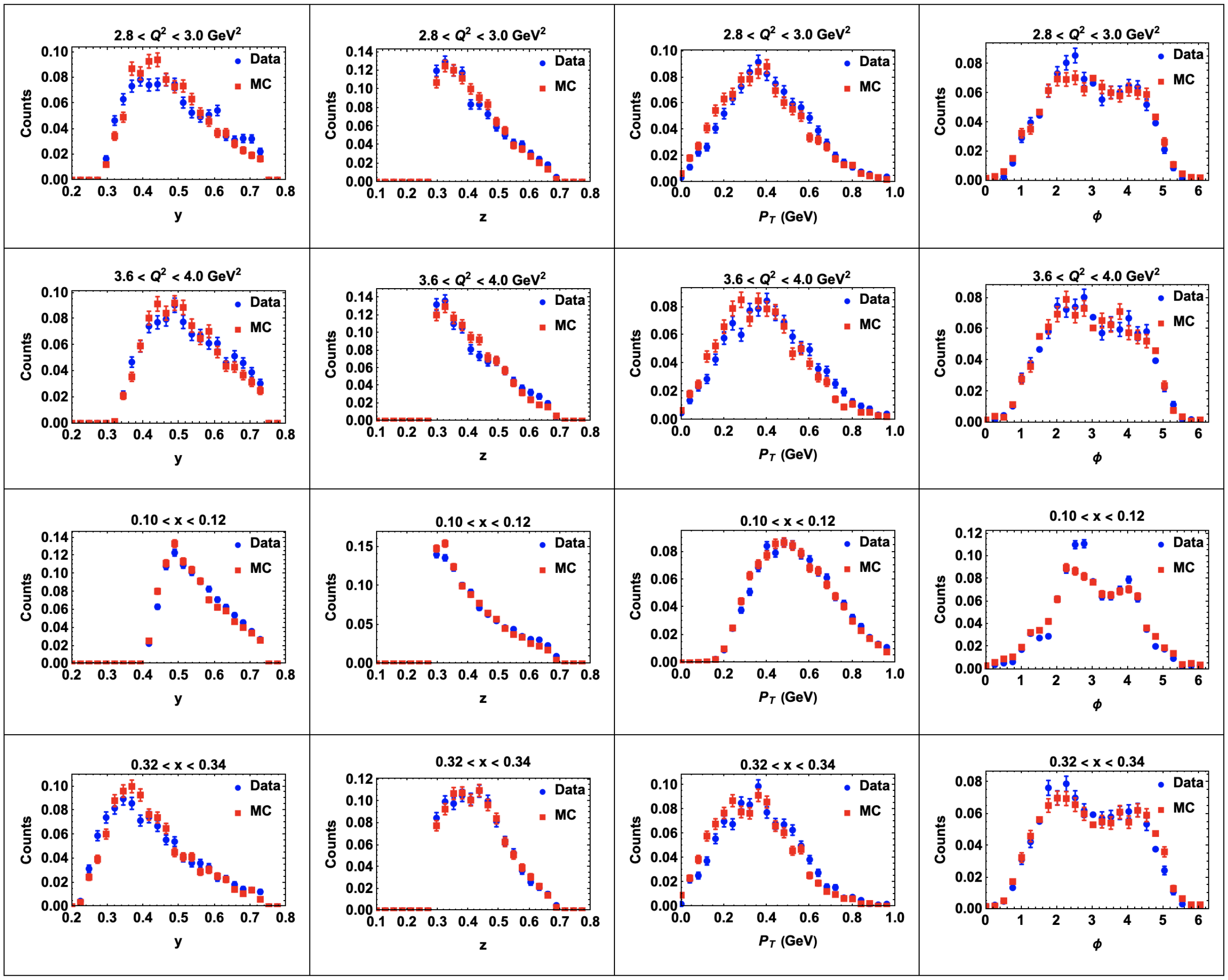

FIG. 5: Comparisons between the integrated outbending 10.6 GeV clasdis MC (red) and RGA Fall18 outbending 10.6 GeV data (blue) samples for y, z, P_T and ϕ without resolution smearing in various bins of Q^2 and x (note that the specific bin $0.32 < x < 0.34$ and $2.8 < Q^2 < 3.0$ is used for statistic projections in the following sections). The datasets have been normalized to the total number of π^+ in order to allow a direct comparison of the shapes of the distributions.

IV. ANALYSIS PROCEDURE

A. Particle Identification and Fiducial Cuts

The particle identification procedure for SIDIS events has been studied extensively in CLAS12 analysis. Similarly, the geometric fiducial cuts necessary to remove detector edge cases, where particle momenta may not be reconstructed accurately, have been thoroughly investigated. We will follow the general outline of previous experiments, allowing for the possibility of slight refinements and adjustments with the forthcoming "pass-2" software and future data requirements. Additional work on the fiducial cuts may be required to ensure that we remain in the well-behaved regions necessary for precise cross section extractions.

B. Channel Selection

For each event, we identify an electron and pion candidate using the particle identification scheme developed for the CLAS12 EventBuilder [45] along with the additional cuts discussed above. The selection of electron and hadron candidates allows for the calculation of various kinematics on an event-by-event basis. The final SIDIS events will be selected with the following list of preliminary cuts.

- $Q^2 > 1.00$ GeV^2, to select DIS events.
- $W > 2.00$ GeV, in order to avoid the resonance region.
- $y < 0.75$, in order to avoid the region most susceptible to radiative effects and the lepton-pair symmetric background (misidentification of the scatterd electron).
- $M_x > 1.50$ GeV, in order to avoid contributions from exclusive production, e.g. $ep \to e'n\pi^+$, $ep \to e'\Delta^0\pi^+$, etc.
- $x_F > 0$, in order to limit contributions from target fragmentation.
- $0.2 \leq z \leq 0.7$ in order to avoid target fragmentation and exclusive channels while focusing on the SIDIS region.

C. Acceptance Correction and Unfolding

The extraction of cross-sections and the Rosenbluth separation analysis for SIDIS require multi-dimensional analysis in (x, Q^2, z, P_T) bins. The acceptance correction procedure will follow a similar approach as the analysis of RGA SIDIS cross-section modulations. The data will be unfolded and corrected for acceptance in multidimensional bins using methods such as Bayesian unfolding. Figure 2 demonstrates the unfolded ϕ spectrum for a fixed (x, Q^2, z, P_T) bin using a 1D migration matrix, which tracks migrations between ϕ bins. The complete 5D unfolding and acceptance correction is currently under investigation and will be implemented accordingly for the proposed studies in this document. In the initial analysis presented in this proposal, a bin-by-bin acceptance correction is utilized.

D. Rosenbluth Separation

Cross sections are estimated for different x-Q^2 bins. For a particular x-Q^2 bin, and for integrated z, P_T and ϕ, the cross sections can be expressed by a constant term G, $K(y)$, and ϵ as

$$\frac{d\sigma}{dxdQ^2dzdP_T} = GK(y)\left(F_{UU,T} + \epsilon F_{UU,L}\right). \tag{11}$$

We use the Rosenbluth L/T separation procedure to further separate $F_{UU,T}$ and $F_{UU,L}$. To perform the Rosenbluth procedure, it is necessary to vary ϵ by keeping Q^2 and x fixed, which can only be done by varying the beam energy. In this proposal, we will use three beam energies of 6.535, 7.546, and 8.4 GeV from the RG-K outbending (positive torus polarity) run and 10.6 GeV from the RG-A outbending run. The procedure to extract $F_{UU,T}$ and $F_{UU,L}$ is then to fit a straight line to the extracted $F_{UU,T} + \epsilon F_{UU,L}$ values for different ϵ points at each fixed Q^2 and x point. The intercept at $\epsilon = 0$ yields $F_{UU,T}$, and the slope gives $F_{UU,L}$.

The procedure for L/T separation was first tested with MC data sets for 6.535, 7.546, 8.4 and 10.6 GeV beam energies. MC banks include the information on the integrated over the whole covered kinematics cross sections, allowing one to define integrated cross sections in any given bin. With the observed resolutions in the kinematic variables, the choice of a 0.02 step in x and 0.2 in Q^2 was tested (still a factor of 4-5 better than the resolutions of CLAS12 expected from MC). The distributions of electron angles and energies in CLAS12 for a given bin ($0.3 < x < 0.32$, $2.8 < Q^2 < 3.0$, $0.2 < z < 0.7$,

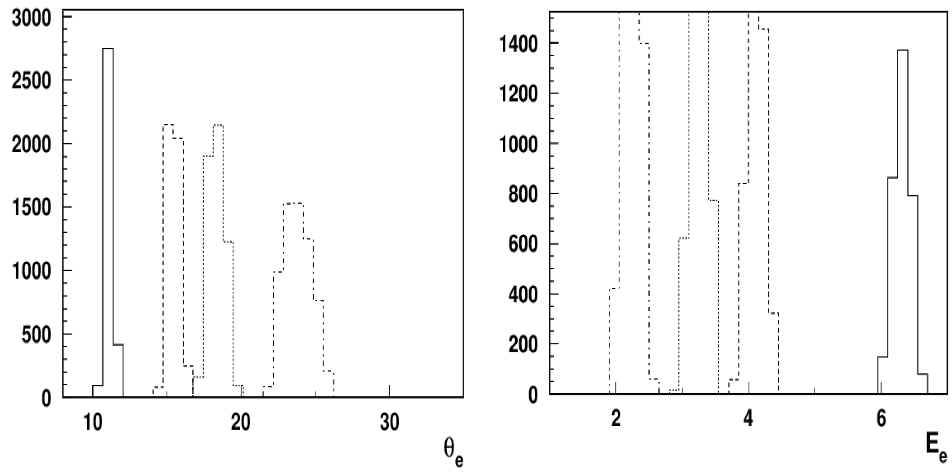

FIG. 6: Distributions of scattered electrons angles (left) and momenta (right) for 4 beam energies for a bin ($0.3 < x < 0.32$, $2.4 < Q^2 < 2.6$, $0.2 < z < 0.7$, and $0.2 < P_T < 0.6$). The solid line is for the beam energy 10.6 GeV, dashed for 8.4 GeV, dotted 7.5 GeV and dash-dotted for 6.535 GeV

and $0.2 < P_T < 0.6$) are shown in Fig. 6, 7. The resolution of the CLAS detector allows for the selection of very small bins in x and Q^2, and the bin sizes in x and Q^2 were chosen to be much less than the corresponding resolutions of CLAS12 (see Fig. 8-9).

The distributions of $e'\pi^+X$ events over the variables y and ϵ are shown in Fig. 10. They were used to calculate the kinematic factors and extract the part of the cross section that depends on the SFs.

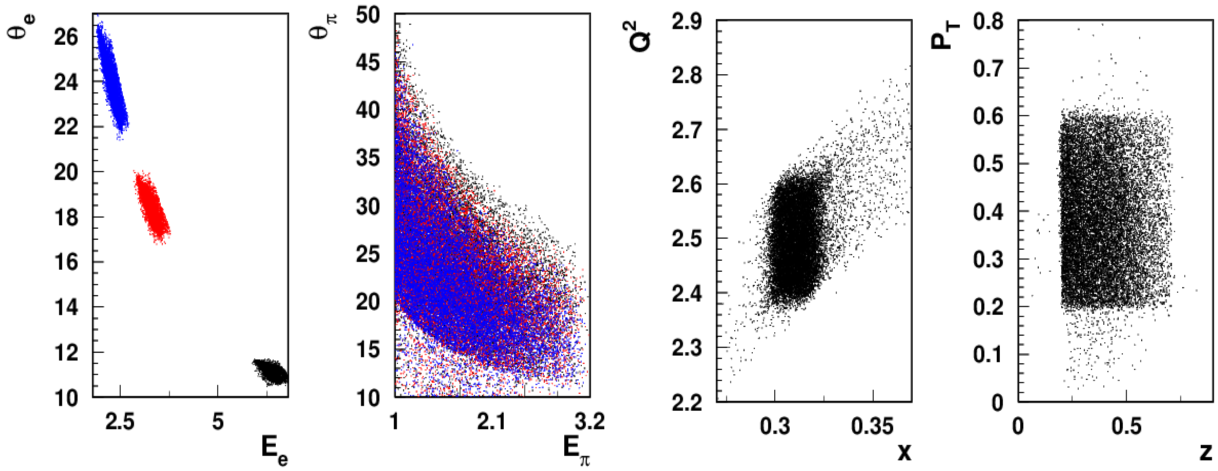

FIG. 7: Distributions of scattered electrons and final state π^+ in momenta and angles (left), and in x vs Q^2 and pion z vs P_T (right) and momenta (right) for 3 beam energies for a bin ($0.3 < x < 0.32$, $2.4 < Q^2 < 2.6$, $0.2 < z < 0.7$, and $0.2 < P_T < 0.6$). The black dots are for 10.6 GeV, red for 7.5 GeV, and blue for 6.535 GeV

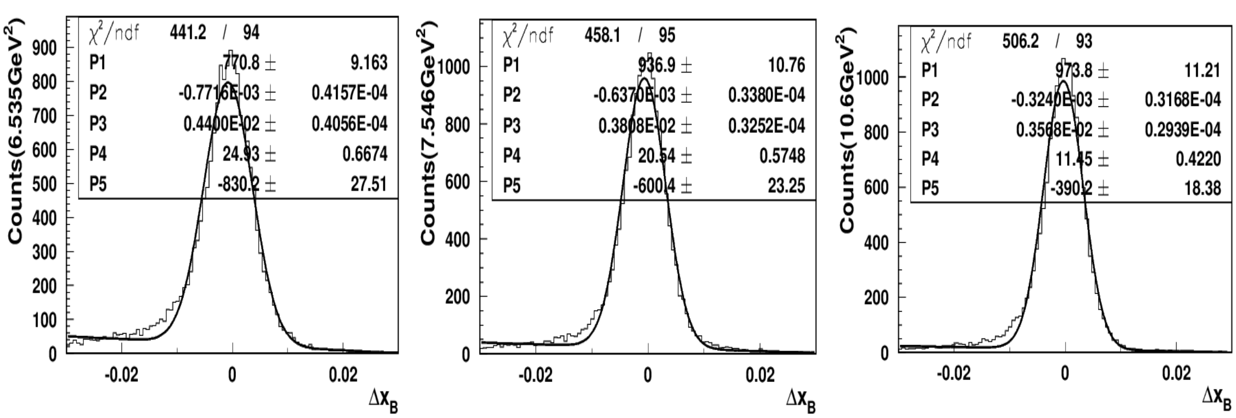

FIG. 8: Resolutions in x-Bjorken for the x-bin $0.3 < x < 0.32$, $2.4 < Q^2 < 2.6$ for different beam energies. Fit was performed using Gauss + first order polinom, so P3 gives the resolution.

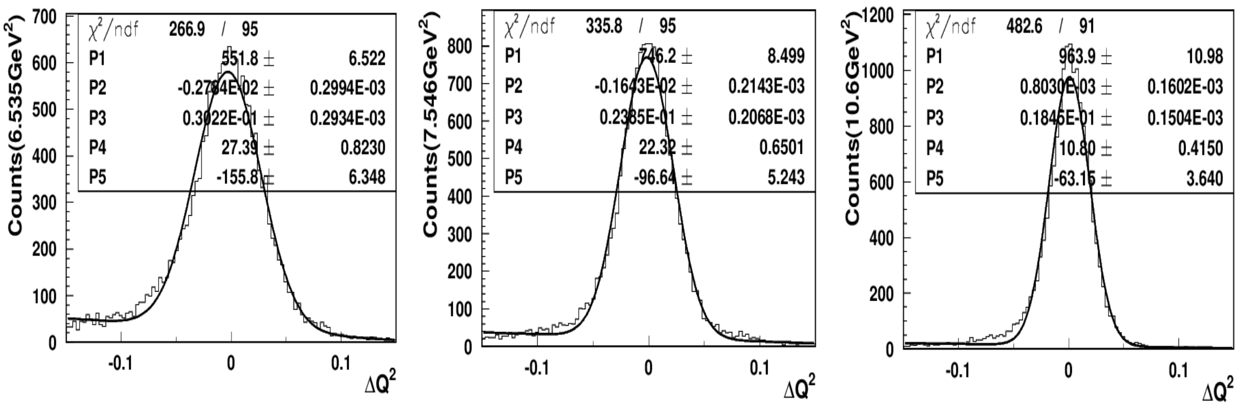

FIG. 9: Resolutions in Q^2 for the x-bin $0.3 < x < 0.32$, $2.4 < Q^2 < 2.6$ for different beam energies. Fit was performed using Gauss + first order polinom, so P3 gives the resolution.

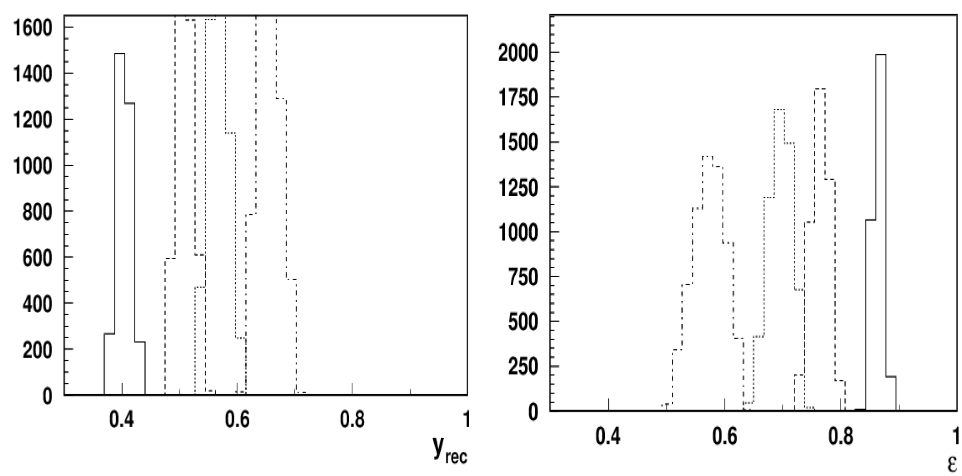

FIG. 10: Distributions of scattered electrons for $y = \nu/E$ (left) and ϵ (right) for 4 beam energies for a bin ($0.3 < x < 0.32$, $2.4 < Q^2 < 2.6$, $0.2 < z < 0.7$, and $0.2 < P_T < 0.6$).

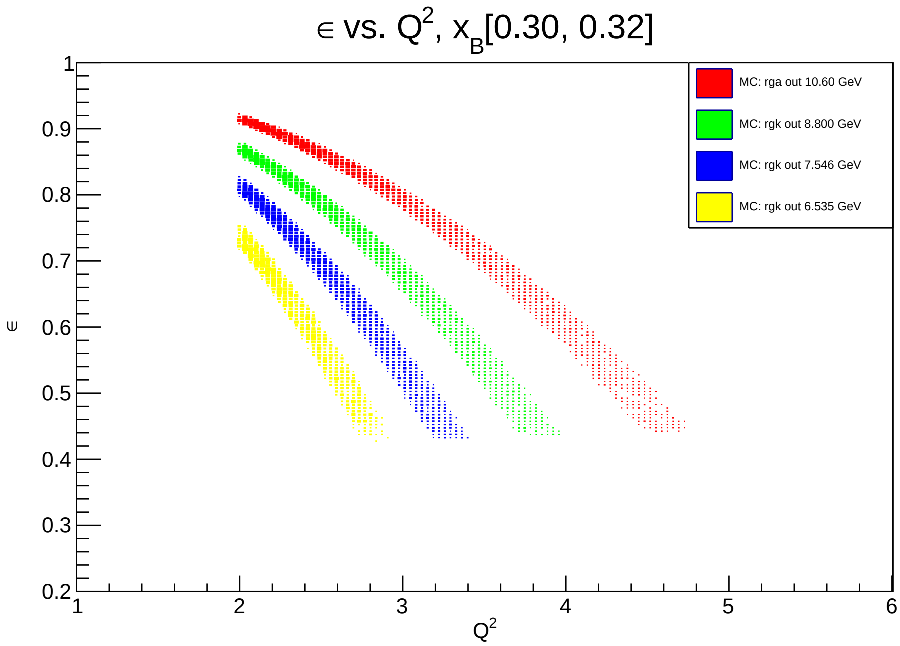

FIG. 11: The ϵ-term as a function of Q^2 for all four beam energies in the outbending torus polarity configuration for the given x_B bin.

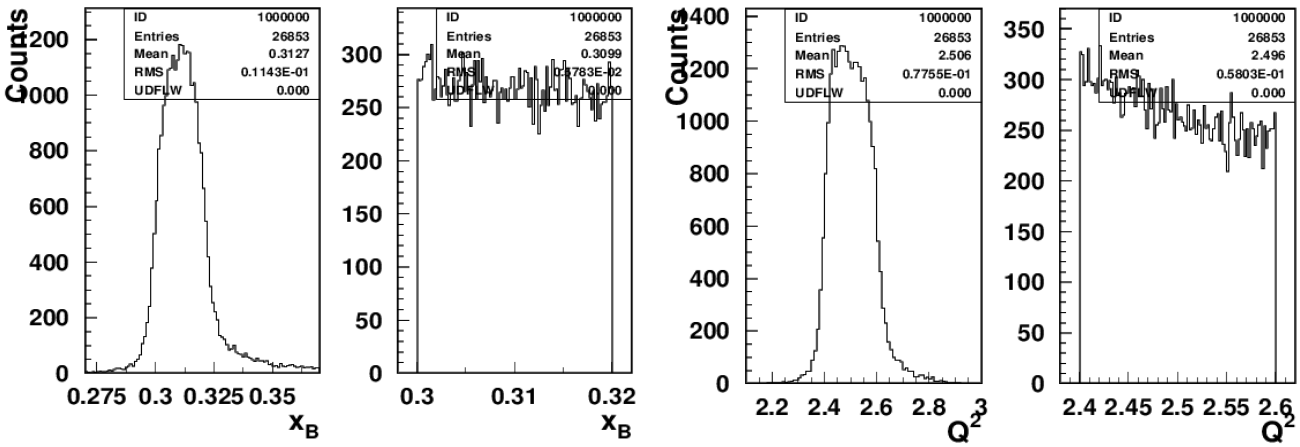

FIG. 12: Generated events corresponding to events reconstructed in bins (sharp edges) in x (left) and Q^2 (right) for 10.6 GeV outbending MC data. Average values for generated x and Q^2 are 0.313, 2.51 with corresponding values in reconstructed bins 0.310, 2.50

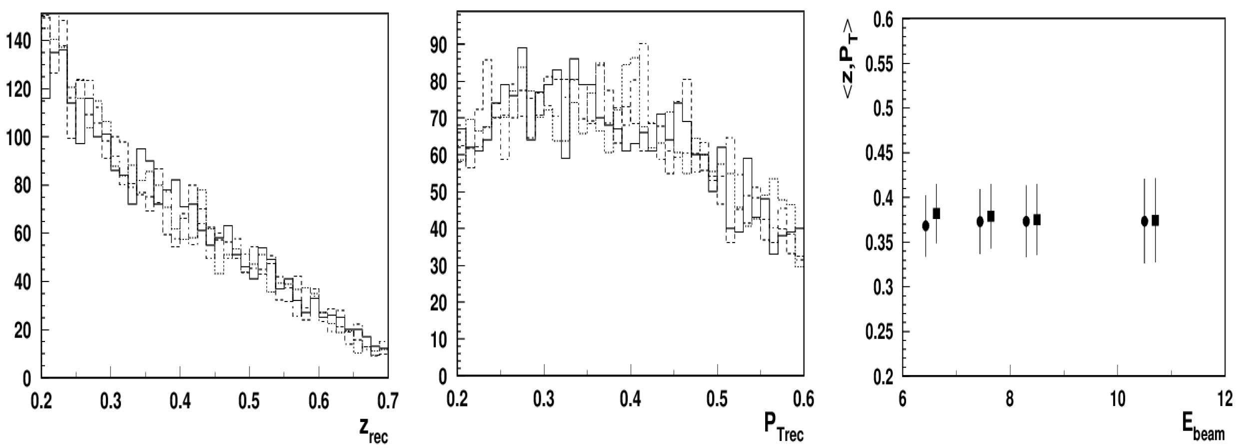

FIG. 13: z (left) and P_T (middle), normalized to same number of events, distributions of $ep \to e'\pi^+X$ events in a given bin from Figs. 6,10. The right panel shows the averages of z (circles) and P_T (squares) vs beam energy.

Although there is some bin migration due to energy loss and detector resolutions, the average values of x and Q^2 reconstructed within bin limits are within 1% consistent with generated averages in the same bin limits (see Fig. 12). The distributions over the π^+ variables z and P_T for all beam energies, shown in Fig. 13, are similar, and were checked to have averages within 1-2%.

The average values of ϵ and the kinematic factor $K(y)$ are shown in Fig. 14. The dependence of the cross section scaled with the value of the kinematic factor $K(y)$ (Fig. 15) is expected to have the beam energy dependence localized only in the term $\epsilon F_{UU,L}$ and can be used to extract the ratio

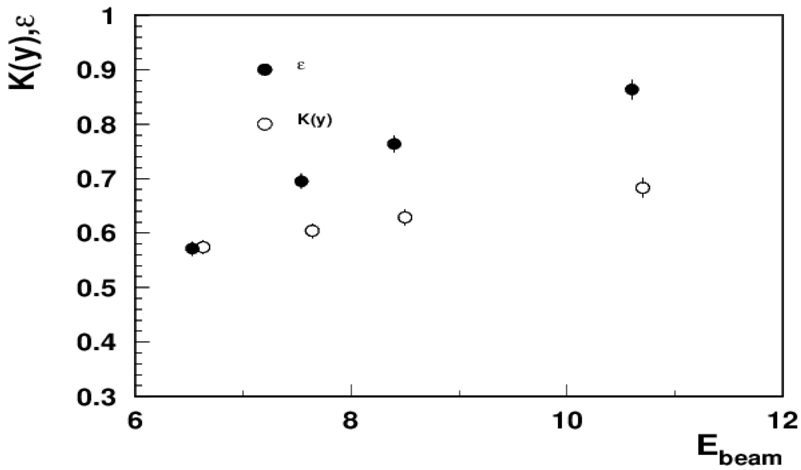

FIG. 14: Dependencies of ϵ and $K(y)$ on the beam energy in a given bin from Figs. 6,10.

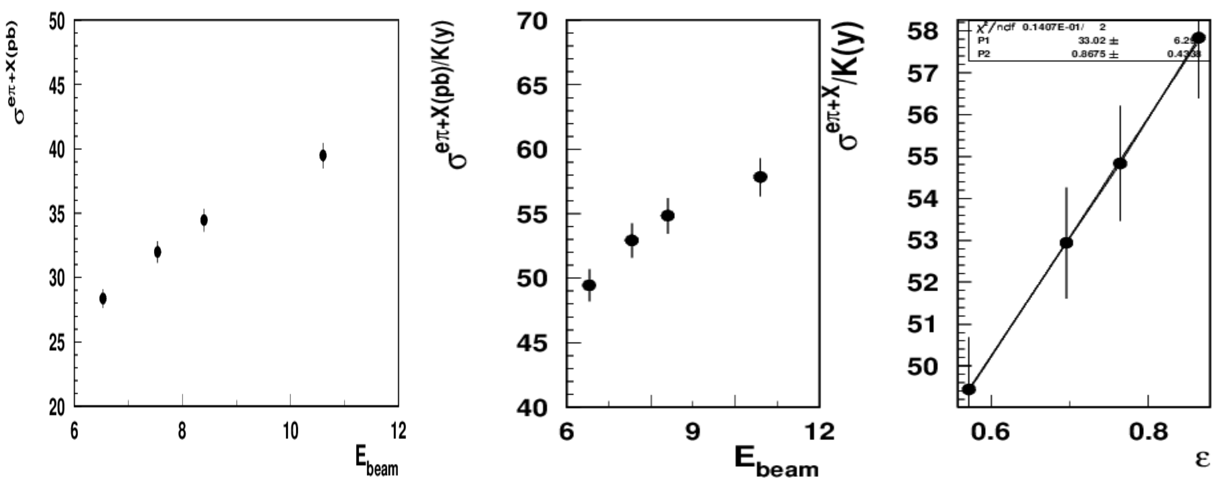

FIG. 15: The integrated cross section in a given bin as a function of the beam energy (left), the same cross section scaled by the energy-dependent kinematic factor K(y) (middle) for a single bin (see Figs6-14). The normalized by the kinematic factor cross sections for $ep \to e'\pi^+X$, was fitted with a linear function $P_1(1+\epsilon P_2)$, with $R = P_2$ (right).

R. R is not supposed to depend on the beam energy, neither $F_{UU,T}$ nor $F_{UU,L}$, and can be checked using different energy settings. The value of R has been recovered from the MC simulation (PEPSI with R=0.8, using the standard LEPTO option for the dynamical higher twist with $R \sim 1/Q^2$ and independent of hadron type and kinematics), for the given bin for $e\pi^+X$ (Fig. 15 and for $e\pi^-X$ (Fig. 16).

While the longitudinal photon contributions entering in the cross sections are expected to be canceled in average in the multiplicities integrated over hadronic variables, the presence of strong

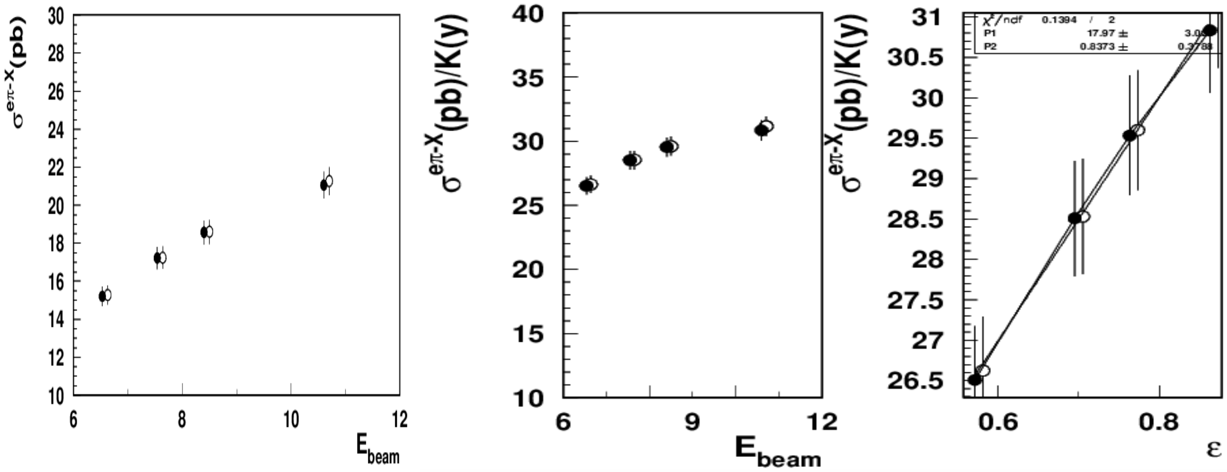

FIG. 16: The integrated cross section in a given bin as a function of the beam energy (left), the same cross section scaled by the energy-dependent kinematic factor K(y) (middle) for a single bin (see Figs6-14). The normalized by the kinematic factor cross sections for $ep \to e'\pi^- X$, was fitted with a linear function $P_1(1+\epsilon P_2)$, with $R = P_2$ (right). Open symbols show the scaled eX cross section and corresponding fit.

kinematic dependence, in particular dependence on the hadron transverse momentum, will create significant contributions in certain phase space. Since most SSAs were observed so far at relatively large z, and show a significant increase in the P_T of hadrons, measurements of kinematic dependencies of R in SIDIS may play a critical role in interpretation of SIDIS at large transverse momenta. That is exactly the kinematics where the TMD theory has major problems in interpretation of the SIDIS data. The ratio R may have significant dependence on z and P_T, possibly increasing quadratically. Since R measured in DIS, which can be considered as an integrated over the z, P_T and ϕ SIDIS summed over all hadrons, it is expected that it will be $\sim$ 15-20%, given the average values of z and P_T in SIDIS experiments are $\sim$ 0.4, at large P_T ($P_T > 0.8$ GeV) and large z the R in SIDIS can be bigger than unity [46]. The superior resolutions of the CLAS12 detector in hadron z and P_T would allow studies of the $R_{\rm SIDIS}$ in a wide kinematic space, allowing detailed measurements of R versus Q^2, z and most importantly P_T of different flavors of hadrons. The resolutions in z and P_T for a given small bin in x and Q^2 are shown in Figs. 17,18.

A similar procedure will be applied to the RGK (6.5,7.5) and RGA (10.6) data combined with future planned RGK measurements with a 8.4 GeV beam. At higher Q^2, the polar angles of the electrons for low beam energies approach the upper limit of the CLAS acceptance. In addition, y at the lowest beam energy 6.535 GeV moves above 0.8, into the region contaminated with photoproduction

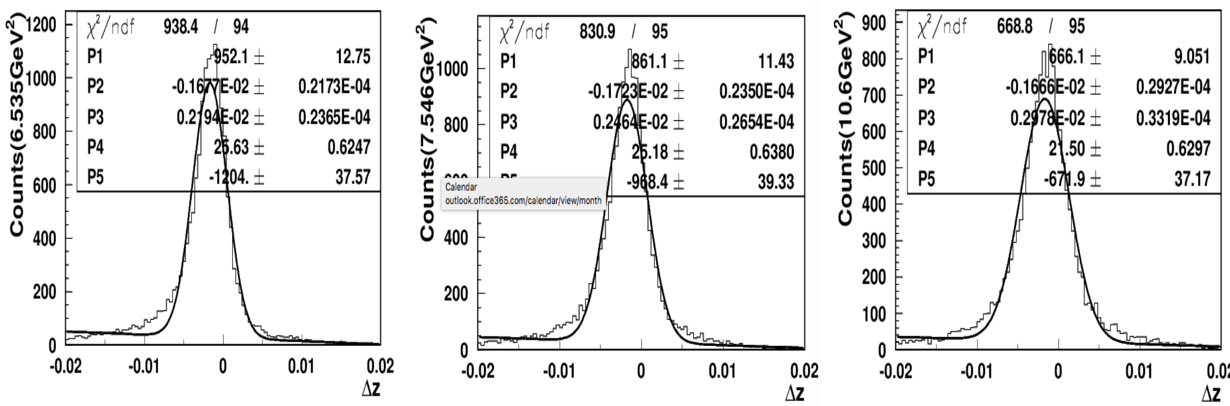

FIG. 17: Resolutions in pion z for the x-bin $0.3 < x < 0.32$, $2.4 < Q^2 < 2.6$ for different beam energies. Fit was performed using Gauss + first order polynomial, so P3 gives the resolution.

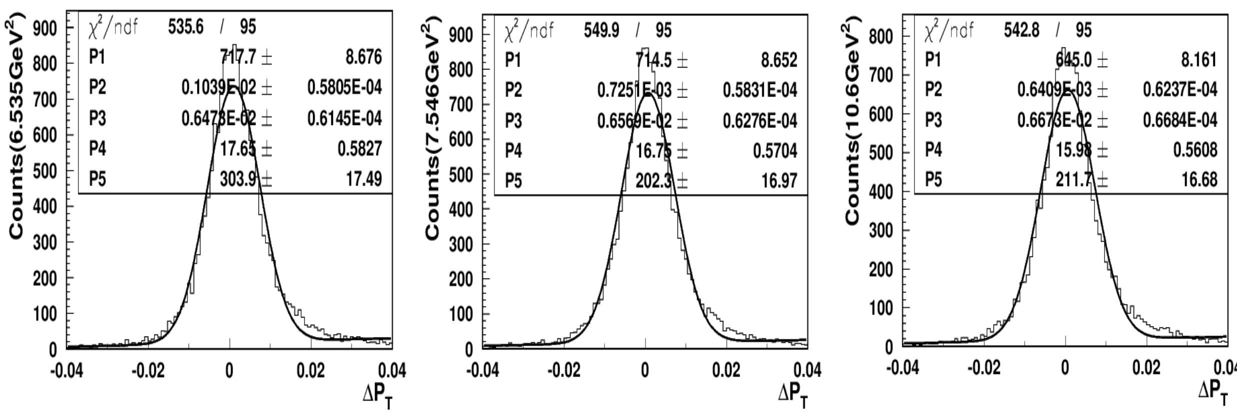

FIG. 18: Resolutions in pion P_T for the x-bin $0.3 < x < 0.32$, $2.4 < Q^2 < 2.6$ for different beam energies. Fit was performed using Gauss + first order polynomial, so P3 gives the resolution.

and large radiative corrections. The values of ϵ and the cross sections for the beam energies 7.546, 8.4, and 10.6 for the higher Q^2 bin are shown in Fig. 19. Above Q^2=3.5 GeV^2, with y for the 7.5 GeV setting, also getting above 0.8, the 8.4 GeV data will be the only available data to be combined with 10.6 for L/T separation (see. Fig. 20). Keeping the systematics below 5% for this measurement will be very important to get a reliable R.

Since systematics will be the dominant factor in the measurements of R, independent measurements with different combinations of beam energies will be very important. Precision cross section measurements ($\sim$ 1.4%) planned at Hall-C (E12-06-104) using HMS and SHMS spectrometers at energies 6.6, 8.8 and 11.0 GeV, with high currents (50 A) on LH2 and LD2 targets will provide an important cross-check and help to validate CLAS12 results in the low P_T region. An important advantage of CLAS12 is the capability to take multiparticle final-state measurements, which will be

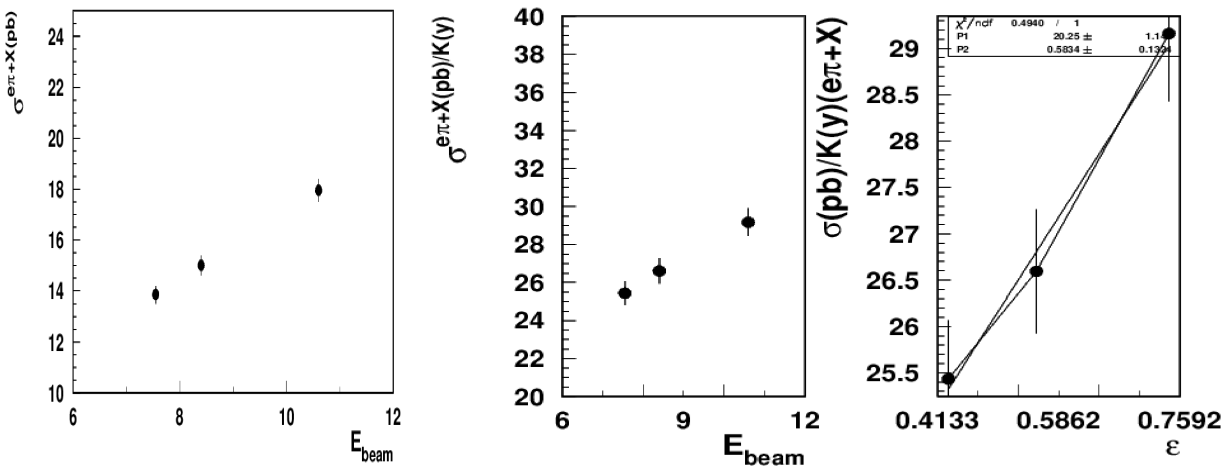

FIG. 19: The integrated cross section in a given bin as a function of the beam energy (left), the same cross section scaled by the energy-dependent kinematic factor K(y) (middle) for a higher Q^2 bin $3.2 < Q^2 < 3.4$. The normalized by the kinematic factor cross sections for $ep \to e'\pi^+X$, was fitted with a linear function $P_1(1+\epsilon P_2)$, with $R = P_2$ (right). The value of R is 0.6 for the average Q^2 of 3.3 GeV^2.

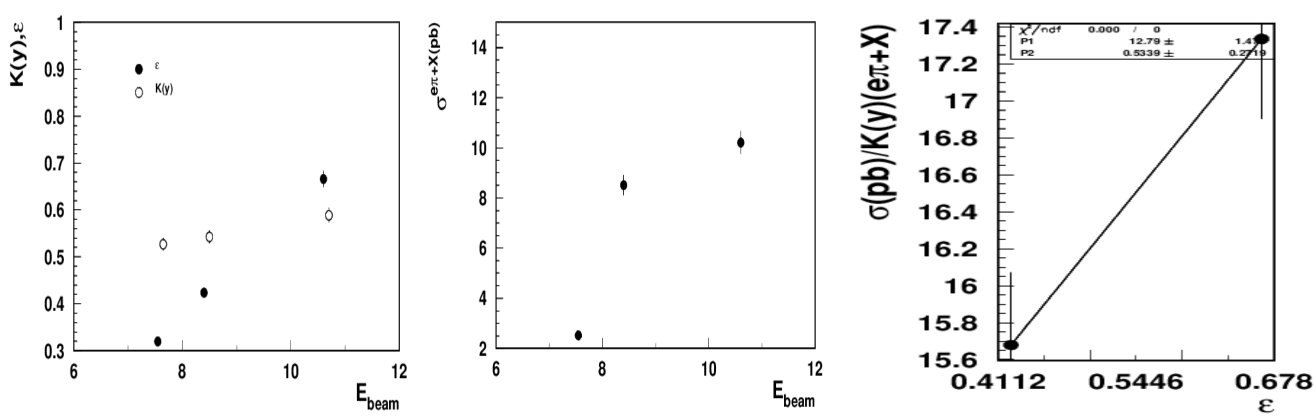

FIG. 20: The ϵ and K(y) (left), the integrated cross section in a given bin as a function of the beam energy (middle), and the fit results for 2 beam settings (right) for a higher Q^2 bin $3.6 < Q^2 < 3.8$. The normalized by the kinematic factor cross sections for $ep \to e'\pi^+X$, was fitted with a linear function $P_1(1+\epsilon P_2)$, with $R = P_2$ (right). The value of R is 0.53 for the average Q^2 of 3.7 GeV^2.

crucial to sort out contributions to pion samples from different processes with very different fractions of $F_{UU,L}$ creating strong kinematic dependences. The distributions of 2-pion samples versus the invariant mass in a given bin in x and Q^2 are shown in Fig. 21. The large $M_{\pi\pi}$, where direct pions start to dominate, corresponds to a large P_T-range where the contributions from vector mesons are expected to be negligible [47].

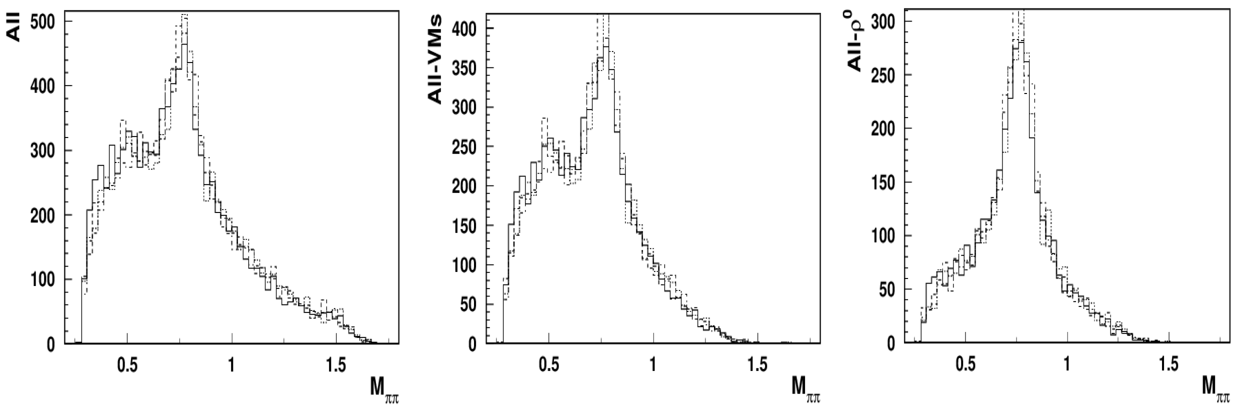

FIG. 21: Distributions of $\pi^+\pi^-$ events as a function of their invariant mass, M_h, for the total sample (left) the sample with one of the pions from a VM decay (middle) and when one of the pions is from ρ^0 (right). Solid line is for 10.6, dashed 8.4, dotted for 7.546, and dashdotted for 6.535.

The fractions of pions coming from VM decays, where they can actually be identified, are very significant (see Figs.22 and 24), indicating that the fraction of pions coming from VM decays will be very high in the inclusive SIDIS ($ep \to e'hX$) and precision measurements of dihadrons will be critical for interpretation of SIDIS data collected so far. The corresponding distributions of 2 pions in z and extracted R are shown in Fig. 23.

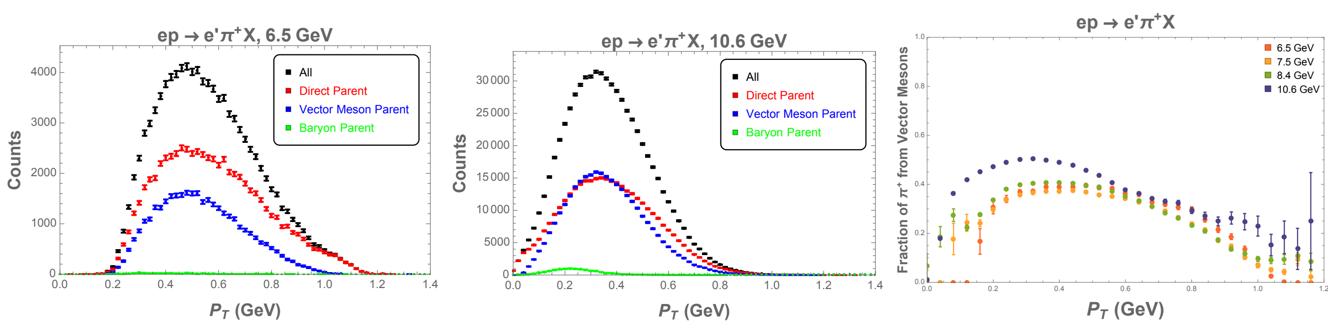

FIG. 22: The P_T distribution for all π^+ (black), π^+ directly produced from the struck quark (red), π^+ from a vector meson parent (blue) and π^+ from a baryon parent (green) for 6.5 GeV (left) and 10.6 GeV (middle) and the fraction of π^+ coming from a vector meson parent as a function of P_T for all four beam energies (right).

Combination of the precision Hall C, and wide acceptance CLAS12, measurements would allow evaluation of R -SIDIS in a wide kinematic range in x, Q^2, z, P_T and for a variety of single and dihadron processes, allowing for the first time to evaluate systematic errors in phenomenological studies disregarding the longitudinal photon contributions.

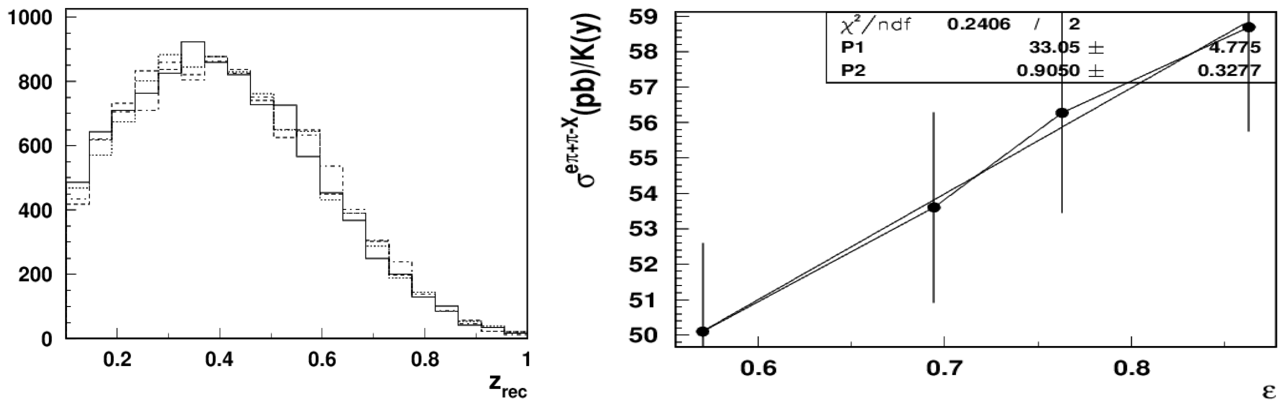

FIG. 23: The z-dependence for different energies (left) and extracted R for the dihadron sample integrated over z and M_h

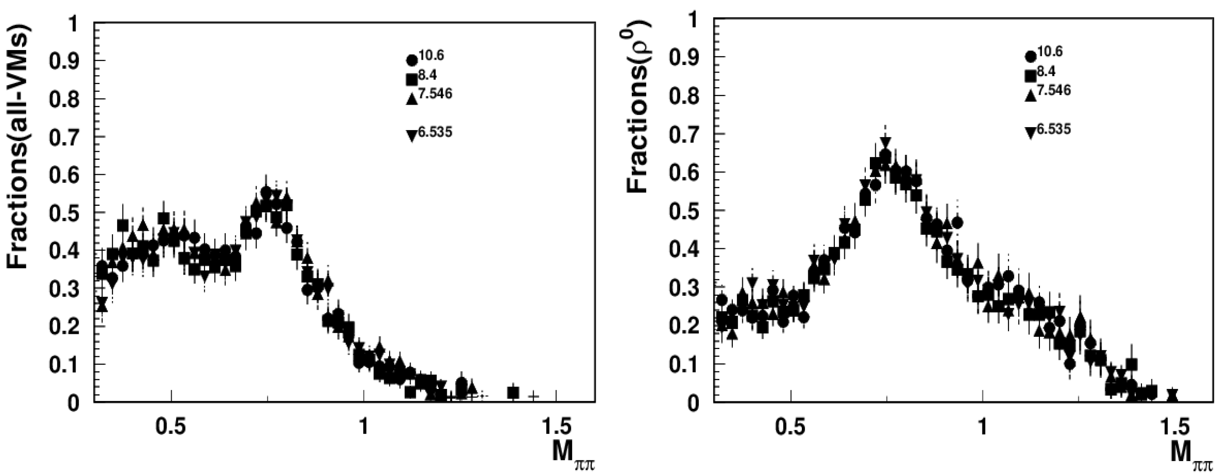

FIG. 24: Fractions of vector meson contributions to overall 2 pion samples. Left panel shows the ratio of events with both pions coming from VM decays to the total number of 2 pion events. The right panel shows the ratio of 2 pion events, when 1 of them is coming from the decay of ρ^0.

V. SYSTEMATIC UNCERTAINTIES

A. Minor Systematic Uncertainties

Different sources of systematic uncertainty have been evaluated and were found to be small. First the effect of PID related contamination of the SIDIS sample were found to be well under control. With a cut on $p < 5$ GeV (or corresponding z cuts to account for the separate beam energies) and additional cuts on the χ^2 value from the PID system, the kaon contamination in the pion sample is in the order of 1 - 2% for most kinematic bins. After a cut on $M_X > 1.5$ GeV, the contamination from baryon resonances is also well under control and at the level of a few percent for most kinematic bins. With a cut on $y < 0.75$ the contamination from charge symmetric background was found to be less than 1% for most kinematic bins.

B. Acceptance Correction

Different acceptance correction methods have been compared. It was found that the results from the different methods agree well, and after a further tuning of the simulations, an uncertainty of a few percent can be assumed for this source. However, compared to the other uncertainties, this source is expected to be one of the major contributions to the systematic uncertainty.

C. Radiative Effects

Radiative photons emitted in the scattering process modify the reconstructed virtual photon's 4-momentum. This introduces a bias in the SIDIS event kinematics that needs to be corrected for. The radiative corrections (RC) for the inelastic part of the SIDIS cross section, due to the production of multiple final-state hadrons, are expected to be more suppressed than the case for inclusive deep-inelastic scattering. The cut in the energy of the virtual photon relative to the incoming electron ($y < 0.75$) was imposed to further suppress the RC. However, the radiative corrections can be significant, in particular at large P_T.

Various methods involving the evaluation of Monte Carlo simulations using the dedicated software (RADGEN) in combination with LEPTO have been used in previous CLAS12 SIDIS measurements.

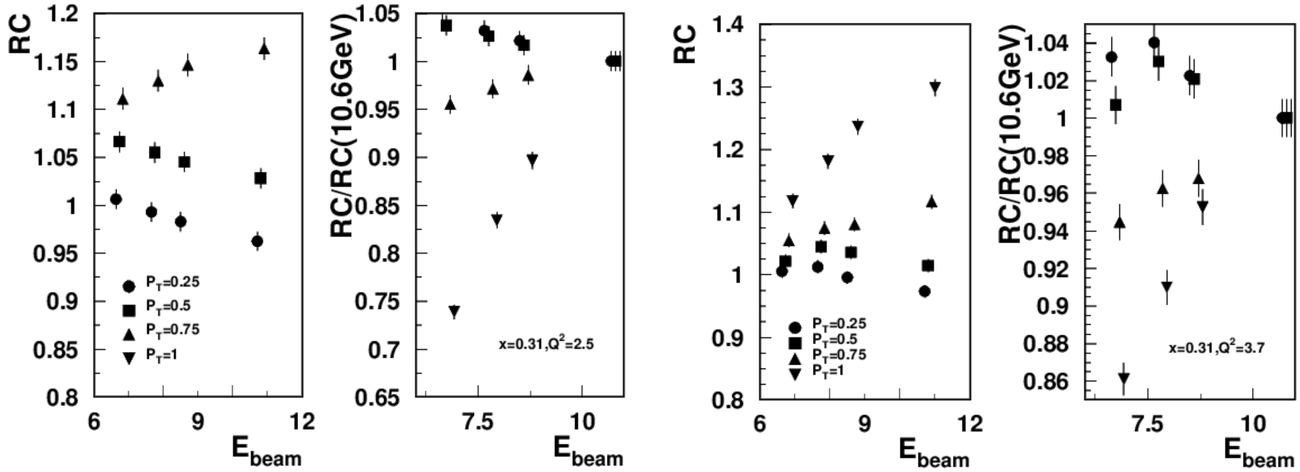

FIG. 25: Radiative corrections (RC=σ_R/σ_B) to SIDIS cross section (left panel) and RC relative to values at 10.6 GeV (right panel) for two bins with $Q^2 = 2.5$ (left) and $Q^2 = 3.7$ (right) for the same $x = 0.31$ bin calculated at $z = 0.4$.

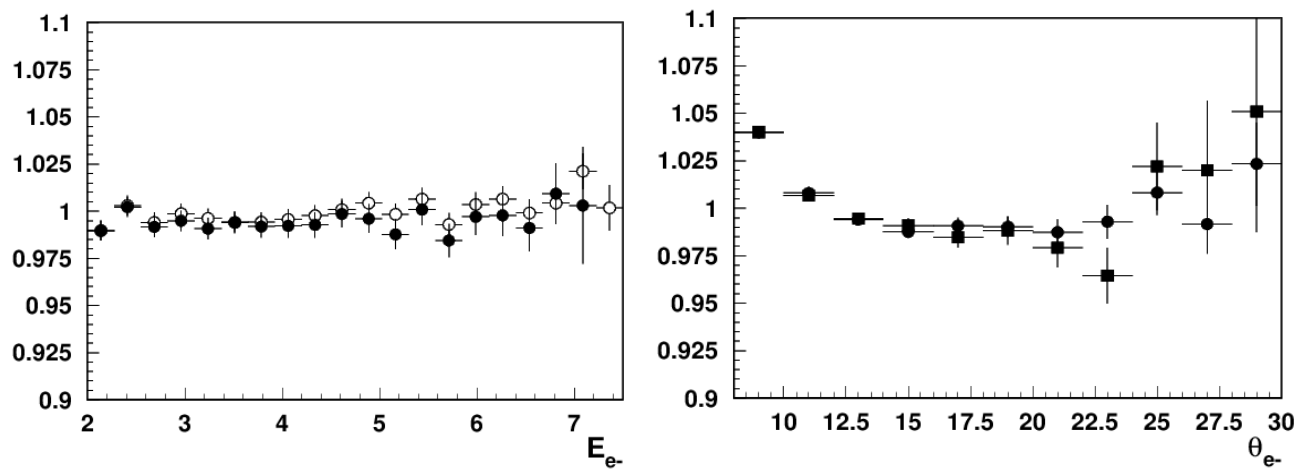

FIG. 26: Ratios of normalized counts of electrons for low lumi (5nA) and high lumi (45nA) runs versus the momentum and polar angle of electrons.

RC values for the bins of interest were studied using the HAPRAD program [48, 49]. As shown in Fig. 25 the RC at large P_T can be very significant, in particular when the missing mass of the $e\pi^+X$ system is approaching the exclusive limit (ex., $P_T \sim 1$ GeV for the $x = 0.31, Q^2 = 2.5$ bin). However, the relative corrections within the phase space used for the L/T separation remain below 5%. The large P_T for the lower Q^2 bin, where the missing mass of the $e\pi^+X$ system is 1.2 GeV, is excluded by our selection cuts requiring $M_X > 1.5$ GeV. The lower energies for the higher Q^2 bin are also excluded, due to our requirement for inelasticity ($y < 0.75$).

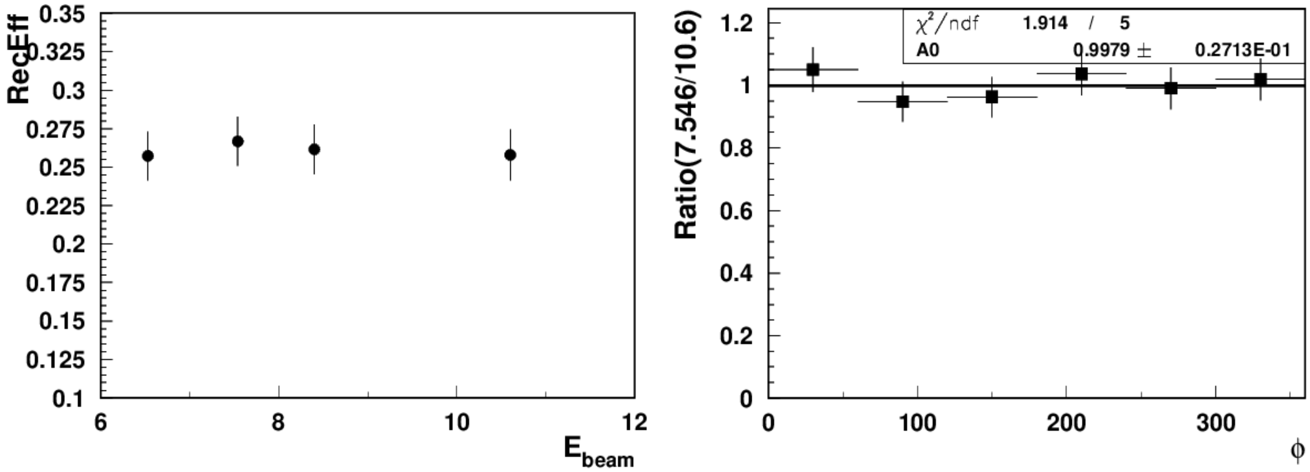

FIG. 27: Reconstruction efficiencies from MC (left), and corrected yields from data, showing normalized to the same counts, dependence on azimuthal angle of electrons (sector dependence).

In addition to standard RC calculations, it is also necessary to consider possible effects from two-photon exchange (TPE) contributions. Their calculation depends on the hadronic structure and requires modeling of the underlying physics. In recent calculations performed for SIDIS (A. Afanasev, S. Lee, private communication), a di-quark model was used for TPE calculation in an approach similar to exclusive pion production [50]. As a result, it was found that epsilon-slope of TPE correction to σ_T can partially mimic, at a few per cent level, effects of σ_L in SIDIS cross sections. After extensive modeling, these effects will be included in evaluation of systematic corrections for the proposed measurements.

D. Total systematic uncertainty

The high lumi background reduces the reconstruction efficiency of the charged tracks. Comparison of low- and high-lumi run collected by CLAS12 demonstrated that the variation of the efficiency of reconstruction has very little kinematic dependence, in particular in the range of momenta and angles of electrons we are interested in (see Fig. 26).

One of the main contributions to overall systemic uncertainty at CLAS12 is the sector dependence. The ratio of contributions for different energies is expected to be smaller (see. Fig. 27). We expect the total systematic uncertainty to be below 5%.

VI. CONCLUSIONS

In SIDIS, a set of independent structure functions are used to characterize the production of hadrons, based on the polarization of the beam and target. The structure functions related to longitudinal photon contributions introducing systematic uncertainties in phenomenological studies, so far neglecting them, can only be evaluated through direct measurements. This will help to validate and improve our understanding of parton dynamics in SIDIS reactions and shed light on various phenomena such as SIDIS multiplicities and variety of SSAs measured in polarized SIDIS in the last 20 years. SIDIS measurements, so far, have relied on the assumption that $R_{\text{SIDIS}} = R_{DIS}$, which introduces considerable uncertainties when using SIDIS data to deduce the flavor and spin distributions of the quarks. Our study is designed to fill this knowledge gap by providing valuable insights into the nucleon structure and quark-gluon dynamics through direct measurements of R_{SIDIS}.

Our proposed addition to the Run Group K experiments aims to provide an in-depth analysis of semi-inclusive deep inelastic scattering (SIDIS) cross sections for single and dihadron production in SIDIS ($ep \to e'hX$ and $ep \to e'hhX$). By combining the RGK data with those from RGA and performing a Rosenbluth separation from measurements at different ratios of the longitudinal and tangential photon flux we will be able to disentangle the separate contributions to the SIDIS cross section for different bins in x, Q^2, and P_T. Comparison of different combinations of beam energies would allow a better evaluation of the systematic errors in the extraction of R, which will be dominated mainly by systematics. For higher Q^2 the new RGK measurements with 8.4 GeV beam will be critical. Our results will extend in phase space future measurements of R, planned at Hall-C, in particular, to higher transverse momenta of final-state hadrons, combining high-precision measurements at Hall-C with wide acceptance measurements with CLAS12. In addition, proposed measurement of dihadron channels would allow us to separate different contributions, and locate the processes most sensitive to longitudinal photon contributions, crucial for proper interpretation of all kind of SSAs observed in SIDIS.

This research will not only contribute to a more accurate and comprehensive understanding of the nucleon structure but also help to refine existing theoretical models and calculations. Direct measurement of R_{SIDIS} will allow more precise determinations of quark distributions and their interactions within the nucleon, providing critical input for the evaluation of systematics in phenomenological studies. The experimental program proposed here is complementary and synergistic with future SIDIS studies at JLab (including SoLID) and the future EIC.

ACKNOWLEDGEMENTS

We thank A. Accardi, I. Akushevich, A. Bacchetta, D. Carman, A. Ilyichev and A. Vladimirov for stimulating discussions and contributions.

---

[1] M. Anselmino, A. Mukherjee, and A. Vossen, "Transverse spin effects in hard semi-inclusive collisions," *Prog. Part. Nucl. Phys.*, vol. 114, p. 103806, 2020.

[2] A. Bacchetta, M. Diehl, K. Goeke, A. Metz, P. J. Mulders, and M. Schlegel, "Semi-inclusive deep inelastic scattering at small transverse momentum," *JHEP*, vol. 02, p. 093, 2007.

[3] A. Kotzinian, "New quark distributions and semiinclusive electroproduction on the polarized nucleons," *Nucl. Phys.*, vol. B441, pp. 234–248, 1995.

[4] P. J. Mulders and R. D. Tangerman, "The complete tree-level result up to order 1/q for polarized deep-inelastic leptoproduction," *Nucl. Phys.*, vol. B461, pp. 197–237, 1996.

[5] A. Airapetian *et al.*, "Azimuthal single- and double-spin asymmetries in semi-inclusive deep-inelastic lepton scattering by transversely polarized protons," *JHEP*, vol. 12, p. 010, 2020.

[6] C. Adolph *et al.*, "Measurement of azimuthal hadron asymmetries in semi-inclusive deep inelastic scattering off unpolarised nucleons," *Nucl. Phys. B*, vol. 886, pp. 1046–1077, 2014.

[7] A. Moretti, "TMD observables in unpolarised Semi-Inclusive DIS at COMPASS," *SciPost Phys. Proc.*, vol. 8, p. 144, 2022.

[8] A. Airapetian *et al.*, "Azimuthal distributions of charged hadrons, pions, and kaons produced in deep-inelastic scattering off unpolarized protons and deuterons," *Phys.Rev.*, vol. D87, p. 012010, 2013.

[9] M. Osipenko *et al.*, "Measurement of unpolarized semi-inclusive pi+ electroproduction off the proton," *Phys. Rev. D*, vol. 80, p. 032004, 2009.

[10] S. Diehl *et al.*, "First multidimensional, high precision measurements of semi-inclusive π^+ beam single spin asymmetries from the proton over a wide range of kinematics," 1 2021.

[11] A. Bacchetta, D. Boer, M. Diehl, and P. J. Mulders, "Matches and mismatches in the descriptions of semi-inclusive processes at low and high transverse momentum," *JHEP*, vol. 08, p. 023, 2008.

[12] M. Anselmino *et al.*, "The role of Cahn and Sivers effects in deep inelastic scattering," *Phys. Rev.*, vol. D71, p. 074006, 2005.

[13] A. Bacchetta, V. Bertone, C. Bissolotti, G. Bozzi, M. Cerutti, F. Piacenza, M. Radici, and A. Signori, "Unpolarized transverse momentum distributions from a global fit of Drell-Yan and semi-inclusive deep-inelastic scattering data," *JHEP*, vol. 10, p. 127, 2022.

[14] I. Scimemi and A. Vladimirov, "Non-perturbative structure of semi-inclusive deep-inelastic and Drell-Yan scattering at small transverse momentum," *JHEP*, vol. 06, p. 137, 2020.

[15] A. Kerbizi, X. Artru, and A. Martin, "Production of vector mesons in the String+$^3P_0$ model of polarized quark fragmentation," *Phys. Rev. D*, vol. 104, no. 11, p. 114038, 2021.

[16] T. Liu, W. Melnitchouk, J.-W. Qiu, and N. Sato, "A new approach to semi-inclusive deep-inelastic scattering with QED and QCD factorization," *Journal of High Energy Physics*, vol. 2021, nov 2021.

[17] J. V. Guerrero, J. J. Ethier, A. Accardi, S. W. Casper, and W. Melnitchouk, "Hadron mass corrections in semi-inclusive deep-inelastic scattering," *JHEP*, vol. 09, p. 169, 2015.

[18] C. J. Bebek, A. Browman, C. N. Brown, K. M. Hanson, R. V. Kline, D. Larson, F. M. Pipkin, S. W. Raither, A. Silverman, and L. K. Sisterson, "Charged Pion Electroproduction from Protons Up to Q**2 = 9.5-GeV**2," *Phys. Rev. Lett.*, vol. 37, pp. 1525–1528, 1976.

[19] S.-y. Wei, Y.-k. Song, K.-b. Chen, and Z.-t. Liang, "Twist-4 contributions to semi-inclusive deeply inelastic scatterings with polarized beam and target," *Phys. Rev. D*, vol. 95, no. 7, p. 074017, 2017.

[20] F. D. Aaron *et al.*, "Measurement of the Inclusive e\pmp Scattering Cross Section at High Inelasticity y and of the Structure Function F_L," *Eur. Phys. J. C*, vol. 71, p. 1579, 2011.

[21] Y. Liang *et al.*, "Measurement of R=σL/σT and the separated longitudinal and transverse structure functions in the nucleon-resonance region," *Phys. Rev. C*, vol. 105, no. 6, p. 065205, 2022.

[22] V. D. Burkert *et al.*, "The CLAS12 Spectrometer at Jefferson Laboratory," *Nucl. Instrum. Meth. A*, vol. 959, p. 163419, 2020.

[23] S. Kuhn *et al.*, "Jlab experiment e12-06-109," 2006.

[24] H. Avakian *et al.*, "Studies of spin-orbit correlations in pion electroproduction in dis with polarized hydrogen and deuterium targets," *JLab Experiment E12-07-107*, 2007.

[25] K. Hafidi *et al.*, "Jlab experiment e12-09-007b," 2009.

[26] H. Avakian *et al.*, "Studies of spin-orbit correlations in kaon electroproduction in dis with polarized hydrogen and deuterium targets," *JLab Experiment E12-09-009*, 2009.

[27] S. Niccolai *et al.*, "Jlab experiment e12-06-109a," 2006.

[28] C. Dilks *et al.*, "Studies of dihadron electroproduction in dis with longitudinally polarized hydrogen and deuterium targets," *JLab Experiment E12-09-007A*, 2019.

[29] Y. Sharabian *et al.*, "The CLAS12 high threshold Cherenkov counter," *Nucl. Instrum. Meth. A*, vol. 968, p. 163824, 2020.

[30] M. Ungaro *et al.*, "The CLAS12 Low Threshold Cherenkov detector," *Nucl. Instrum. Meth. A*, vol. 957, p. 163420, 2020.

[31] M. Contalbrigo *et al.*, "The CLAS12 Ring Imaging Cherenkov detector," *Nucl. Instrum. Meth. A*, vol. 964, p. 163791, 2020.

[32] M. D. Mestayer *et al.*, "The CLAS12 drift chamber system," *Nucl. Instrum. Meth. A*, vol. 959, p. 163518, 2020.

[33] D. Carman *et al.*, "The CLAS12 Forward Time-of-Flight system," *Nucl. Instrum. Meth. A*, vol. 960, p. 163629, 2020.

[34] G. Asryan *et al.*, "The CLAS12 forward electromagnetic calorimeter," *Nucl. Instrum. Meth. A*, vol. 959, p. 163425, 2020.

[35] M. Antonioli *et al.*, "The CLAS12 Silicon Vertex Tracker," *Nucl. Instrum. Meth. A*, vol. 962, p. 163701, 2020.

[36] D. Carman *et al.*, "The CLAS12 Central Time-of-Flight system," *Nucl. Instrum. Meth. A*, vol. 960, p. 163626, 2020.

[37] A. Acker *et al.*, "The CLAS12 Micromegas Vertex Tracker," *Nucl. Instrum. Meth. A*, vol. 957, p. 163423, 2020.

[38] M. Ungaro *et al.*, "The CLAS12 Geant4 simulation," *Nucl. Instrum. Meth. A*, vol. 959, p. 163422, 2020.

[39] H. Avakian, "clasdis." `https://github.com/JeffersonLab/clasdis`, 2020.

[40] T. Sjostrand, S. Mrenna, and P. Z. Skands, "PYTHIA 6.4 Physics and Manual," *JHEP*, vol. 0605, p. 026, 2006.

[41] L. Mankiewicz, A. Schafer, and M. Veltri, "PEPSI: A Monte Carlo generator for polarized leptoproduction," *Comput. Phys. Commun.*, vol. 71, pp. 305–318, 1992.

[42] G. Ingelman, A. Edin, and J. Rathsman, "LEPTO 6.5: A Monte Carlo generator for deep inelastic lepton - nucleon scattering," *Comput.Phys.Commun.*, vol. 101, pp. 108–134, 1997.

[43] T. B. Hayward, "Dihadron beam spin asymmetries on an unpolarized hydrogen target with CLAS12." Thesis, College of William & Mary, available at `https://www.jlab.org/Hall-B/general/thesis/THayward_thesis.pdf`, 2021.

[44] CLAS, "11 GeV polarized electrons on liquid hydrogen target to study proton structure, 3d imaging, and gluonic excitations, RG-A analysis overview and procedure." Internal Note, under review. Snap-

shot from August 2020: https://clas12-docdb.jlab.org/DocDB/0009/000949/001/RGA_Analysis_Overview_and_Procedures-08172020.pdf.

[45] V. Ziegler *et al.*, "The CLAS12 software framework and event reconstruction," *Nucl. Instrum. Meth. A*, vol. 959, p. 163472, 2020.

[46] A. Brandenburg, V. V. Khoze, and D. Mueller, "Semiexclusive pion production in deep inelastic scattering," *Phys. Lett. B*, vol. 347, pp. 413–418, 1995.

[47] H. Avakian, "Hadronization of quarks and correlated di-hadron production in hard scattering," *PoS*, vol. DIS2019, p. 265, 2019.

[48] I. Akushevich, N. Shumeiko, and A. Soroko, "Radiative effects in the processes of hadron electroproduction," *Eur. Phys. J. C*, vol. 10, pp. 681–687, 1999.

[49] I. Akushevich, A. Ilyichev, and M. Osipenko, "Complete lowest order radiative corrections to five-fold differential cross-section of hadron leptoproduction," *Phys. Lett. B*, vol. 672, pp. 35–44, 2009.

[50]